Zou, Yibiao; Crowther, Thomas W.; Smith, Gabriel Reuben; Ma, Haozhi; Mo, Lidong; Bialic-Murphy, Lalasia; Potapov, Peter; Gawecka, Klementyna A.; Xu, Chi; Negret, Pablo J.; Lauber, Thomas; Wu, Zhaofei; Rebindaine, Dominic; Zohner, Constantin M. 2025. **Fragmentation increased in over half of global forests from 2000 to 2020**.

Title: Fragmentation increased in over half of global forests from 2000 to 2020

Authors: Yibiao Zou[1*], Thomas W. Crowther[1,2], Gabriel Reuben Smith[1], Haozhi Ma[3], Lidong Mo[1], Lalasia Bialic-Murphy[1], Peter Potapov[4,5], Klementyna A. Gawecka[6,10], Chi Xu[7], Pablo J. Negret[8,11], Thomas Lauber[1], Zhaofei Wu[1,3,9], Dominic Rebindaine[1], Constantin M. Zohner[1]

Affiliations:

[1]Institute of Integrative Biology, ETH Zurich (Swiss Federal Institute of Technology), Universitätsstrasse 16, 8092 Zurich, Switzerland.

[2]Oath, 101 Montgomery Street, The Presidio of San Francisco, CA 94129.

[3]Swiss Federal Institute for Forest, Snow and Landscape Research WSL, 8903 Birmensdorf, Switzerland.

[4]World Resources Institute, Washington, DC, USA.

[5]Department of Geographical Sciences, University of Maryland, College Park, MD, USA.

[6]Department of Evolutionary Biology and Environmental Studies, University of Zurich, Winterthurerstrasse 190, 8057 Zürich, Switzerland.

[7]School of Life Sciences, Nanjing University, Nanjing, China.

[8]Wyss Academy for Nature, Centre for Development and the Environment, Institute of Geography, University of Bern, Switzerland.

[9]College of Water Sciences, Beijing Normal University, Beijing 100875, China.

[10]UK Centre for Ecology & Hydrology, Bush Estate, Penicuik, EH26 0QB, UK.

[11]Hawkesbury Institute for the Environment, Western Sydney University, Australia.

*Corresponding author. Email: yibiao.zou@usys.ethz.ch

Abstract: Habitat fragmentation, where contiguous forests are broken into smaller, isolated patches, threatens biodiversity by disrupting species movement, shrinking populations, and altering ecosystem dynamics. Past assessments suggested declining global fragmentation, they relied on structure-based metrics that overlook ecological connectivity. Here, we analyze global forest fragmentation from 2000 to 2020 using complementary metrics capturing patch connectivity, aggregation, and structure. Connectivity-based metrics reveal that 51–67% of forests globally–and 58–80% of tropical forests–became more fragmented, nearly twice the rate suggested by traditional structure-focused methods (30–35%). Aggregation-focused metrics confirm increases in 57–83% of forests. Human activities such as agriculture and logging drive this change. Yet, protected tropical areas saw up to an 82% reduction in fragmentation, underscoring the potential of targeted conservation.

Main Text:

Introduction

Forests are essential to global biodiversity and climate regulation (*1-6*). Yet, human activities increasingly threaten them, not only by reducing forest area but also by fragmenting forests into smaller, isolated patches (*7-10*). This process, known as habitat fragmentation (hereafter "fragmentation"), reduces species richness and carbon storage (*11-13*). Its importance, particularly regarding ecological connectivity and integrity, is emphasized in global policy frameworks such as the Aichi Target 11 and the Kunming-Montreal Global Biodiversity Framework (*14, 15*). Accurately quantifying fragmentation is critical not only to understand its global extent but also to identify high-risk regions and guide conservation efforts.

Fragmentation arises through multiple pathways: patches may shrink, split, vanish, stretch into complex shapes, or grow more distant (Fig. 1A-E). These changes often co-occur, as in ongoing Amazon deforestation (Fig. 1F & S2), and affect biodiversity through three main mechanisms (*16-21*). First, new edges change microclimates and disturbance regimes, often making forests warmer and drier (*22, 23*). Second, shrinking core areas threaten species dependent on large, intact habitats (*11*). Third, increased patch isolation disrupts connectivity and reduces movement, often leading to long-term population declines (*24-26*). While edge effects vary, losses of core habitat and connectivity consistently harm forest specialists (*11, 17*).

To assess these impacts, researchers use a range of landscape metrics (*27-32*), broadly categorized into structure, aggregation, and connectivity (*7, 11*). Structure-focused metrics quantify habitat subdivision, including patch number, size, and edge length, but often neglect the habitat extent and spatial arrangement (*7*). Aggregation-focused metrics assess how clustered patches are but may also overlook overall extent. Connectivity-focused metrics incorporate both patch area and spatial configuration, offering a more ecologically relevant perspective. Since each captures different aspects of fragmentation, selecting ecologically meaningful metrics is critical to accurately track progress toward conservation goals (*27, 33*).

Connectivity- and aggregation-focused studies suggest that fragmentation has increased in recent decades, particularly in the tropics (*34-36*). For example, Hansen et al. (2020) found consistent tropical forest patch loss from 2001 to 2018, with smaller patches disappearing fastest (*35*). Edge habitat also expanded from 2000 to 2010, increasing exposure to disturbances (*36*). However, global assessments using structure-focused metrics reported declining fragmentation in 75% of forests from 2000 to 2020 (*7*) despite a net forest loss of 101 Mha (*37*). This discrepancy arises because structure metrics define fragmentation by patch number and size, interpreting fewer, larger patches as reduced fragmentation (Fig. 1C, F), even when ecologically critical patches are lost (*7, 33, 38, 39*). Such losses reduce connectivity and harm species that depend on stepping-stone habitats for dispersal and persistence (*11, 13, 19*).

In conservation biology, debate persists over whether habitat configuration (Fig. 1A) or total area plays a greater role in shaping biodiversity (*13, 17-19*). Structure-focused metrics are valuable for isolating the effects of fragmentation *per se*—that is, changes in patch structure without habitat loss (*11, 19*). However, they often overlook critical aspects like connectivity and aggregation, limiting their ability to capture how landscape change affects species movement, resource access, and population viability (*7, 11, 13*). As such, they can misrepresent fragmentation trends over time. A comprehensive global assessment must therefore integrate connectivity- and aggregation-focused metrics to fully reflect fragmentation's ecological impacts and its drivers.

Here, we quantify global forest fragmentation from 2000 to 2020 using a comprehensive set of metrics representing habitat connectivity, aggregation, and structure (Table. 1, Fig. 1 & S1). We calculated nine widely used fragmentation metrics (*7, 27-30, 32*), grouped into three categories based on their ecological

focus. Connectivity metrics included TCA (total core forest area), LPI (largest patch index), and LDI (landscape division index; probability that two randomly placed individuals occur in the same forest patch (*29*)). Aggregation metrics included AI (aggregation index), PLADJ (patch-to-edge length adjacency), and ENN (mean Euclidean nearest neighbor distance among patches). Structural metrics included MPA (mean patch area), ED (edge density), and NP (number of patches) (see Table 1 and Table S1 for detailed description). To capture broader fragmentation trends, we synthesized these into three composite indices: the Connectivity-based Fragmentation Index (CFI), the Aggregation-based Fragmentation Index (AFI) (*27-30, 32*), and the Structure-based Fragmentation Index (SFI, formerly termed the Forest Fragmentation Index (FFI) in ref(*7*)). We first demonstrate how each metric responds to hypothetical and real-world landscape-changes, demonstrating their ecological relevance. We then apply them to high-resolution (30 m) global forest cover data (*37*) to map trends in fragmentation, identify key drivers (*8*), and evaluate the effectiveness of protected areas in mitigating fragmentation.

Results

Fragmentation metrics respond differently to landscape change

Fragmentation metrics responded differently depending on the type of landscape alteration (Fig. 1). All metric groups detected increased fragmentation when forest patches were subdivided without significant forest loss, with structure-focused metrics showing the strongest response to patch division (Fig. 1A). In contrast, connectivity-focused metrics consistently indicated increased fragmentation in scenarios involving shrinking patches (Fig. 1B), the disappearance of patches (Fig. 1C), and real-world deforestation (Fig. 1F). In these cases, structure-focused metrics often suggested reduced fragmentation, highlighting their insensitivity to losses in habitat connectivity. Aggregation-focused metrics were especially responsive to increases in patch shape complexity (Fig. 1D) and patch distance (Fig. 1E), but indicated reduced fragmentation when patches disappeared (Fig. 1C), resulting in variable outcomes in real-world scenarios (Fig. 1F & S2). Notably, only the aggregation-focused ENN and the composite AFI detected increased fragmentation when patch separation increases without loss of area (Fig. 1E), underscoring their unique sensitivity to spatial configuration.

To quantify how these fragmentation dimensions manifest globally, we conducted a Principal Component Analysis (PCA) on all individual and composite metrics. We also incorporated Metapopulation Capacity (MPC)—a measure of functional connectivity reflecting a landscape's ability to support species persistence (*25, 31*). The PCA biplot revealed three statistically distinct metric clusters (MANOVA p-value < 0.001), corresponding to habitat connectivity, aggregation, and structure (Fig. 2A). Connectivity-focused metrics aligned closely with MPC (Fig. 2A, S10C), confirming their strength in capturing functional connectivity and ecologically meaningful fragmentation (Fig. 2A, S10C). This underscores the importance of incorporating connectivity-based approaches in global fragmentation assessments to better understand biodiversity impacts and conservation priorities.

Trends of global fragmentation from 2000 to 2020

To quantify global forest fragmentation trends, we assessed the proportion of forest area showing increased fragmentation from 2000 to 2020 at multiple spatial resolutions (5, 10, 20, and 40 km). We used three composite indices—CFI, AFI and SFI—to capture trends globally and across major forest biomes (tropical, temperate, and boreal). The results reveal stark differences among metric types. The CFI indicates that, depending on grid size, 51-67% of forests globally (Fig. 2C), and 58-80% of tropical forests (Fig. 2D), have become more fragmented. Similarly, the AFI suggests that 57-83% of global forests became more fragmented, reflecting declines in spatial proximity and ecological connectivity, both crucial for species movement and habitat continuity. In contrast, the SFI suggests that only 30-35% of forests

worldwide became more fragmented over the same period (Fig. 2C), aligning with earlier findings (*7*). This discrepancy arises because the SFI interprets the loss of small or connecting patches as reduced fragmentation, due to its focus on patch number and size rather than ecological connectivity.

Fragmentation estimates from the CFI and AFI were scale-dependent, with higher fragmentation detected at coarser resolutions (10–40 km; Fig. 2C–D). This reflects the edge-driven nature of fragmentation: as grid size increases, fewer cells fall within intact cores, increasing the apparent fragmentation rate. By contrast, the SFI remained largely scale-insensitive, even indicating slight declines in fragmentation at larger scales (Fig. 2C-D).

To examine how fragmentation metrics respond to deforestation, we related each composite metric to forest cover at a 5 km resolution for the year 2000 (Fig. 2B) and 2020 (Fig. S5). CFI and AFI values declined with increasing forest cover, aligning with ecological expectations that larger, contiguous forests are less fragmented (*11*). By contrast, the SFI indicated reduced fragmentation in areas with both low and high forest cover, thus equating severe deforestation with reduced fragmentation and highlighting its limitations in capturing deforestation-driven fragmentation. Spatial analysis confirms that these discrepancies between metrics are most pronounced across the pan-tropical regions (Fig. S9), where deforestation is severe (*8, 35*).

Drivers of forest fragmentation

Forest fragmentation and cover loss arise from various processes that can be broadly classified into permanent conversion and temporary disturbances (*8*). Permanent conversion includes commodity-driven deforestation (e.g., mining, energy development) and urban expansion, resulting in lasting land-use change. Temporary disturbances, such as shifting agriculture (agricultural conversion followed by abandonment), forestry (clearcutting or selective logging), and wildfires, often allow for forest regrowth over time.

To quantify the contribution of these drivers, we integrated data from the Global Forest Watch dataset (*8*), which maps primary deforestation drivers from 2000 to 2023 (Fig. 3). Results were consistent with earlier assessments (*8*) from 2000 to 2015 (Figs. S12–S13), confirming the growing influence of anthropogenic disturbance, especially shifting agriculture, commodity-driven deforestation, and forestry. We used the CFI at 5-km resolution (the finest available) for this analysis and the subsequent assessment of protected areas, as it best aligned with ecological indicators of fragmentation (Fig. 2A-B, S10).

Globally, shifting agriculture (37% of grids with increased fragmentation) and forestry (34%) were the dominant drivers of increased fragmentation (Fig. 3), followed by wildfires and commodity-driven deforestation (both 14%). In the tropics, fragmentation was overwhelmingly driven by shifting agriculture (61%), while temperate forests were mainly affected by forestry (81%). In boreal regions, wildfires (62%) and forestry (38%) were the primary drivers. Permanent conversions from commodity-driven deforestation and urbanization accounted for less than 15% of fragmentation globally. Identifying these region-specific drivers is essential for designing targeted and effective conservation strategies.

Fragmentation status within and outside protected areas

To examine how protection status influences forest fragmentation, we integrated data from the World Database on Protected Areas (WDPA) (*40*). Area-based protection remains a cornerstone of biodiversity conservation (*41, 42*), and previous studies suggest that protected tropical forests face fewer human disturbances (*43*). However, whether this translates into reduced fragmentation rates over time remains unclear.

We classified 5-km forest grid cells into protected and non-protected categories and applied a matching approach to control for environmental and socio-economic differences (*42, 44-46*) (Fig. S14–S16). Fragmentation trends from 2000 to 2020 were analyzed across four categories: strictly protected, protected, matched non-protected, and all non-protected. Given distinct fragmentation drivers, tropical

and non-tropical forests were analyzed separately.

In the tropics, fragmentation increased in all categories but remained significantly lower in protected areas. Strictly protected areas experienced 82% less fragmentation than matched non-protected areas, while less strictly protected areas saw a 45% reduction (Fig. 4A). These patterns align with reduced human activity: shifting agriculture was 59% and 16% lower in strictly and less strictly protected areas, respectively, while forestry was 10% and 58% lower (Fig. 4B). These results highlight the effectiveness and importance of tropical protected areas in limiting human-driven fragmentation, and underscore the urgent need to expand protection across tropical regions in line with international conservation targets, including Aichi Target 11 and the "30x30" goal of the Kunming-Montreal Global Biodiversity Framework (*14, 15*).

In contrast, non-tropical forests showed slightly higher fragmentation in strictly protected areas compared to non-protected ones (Fig. 4C), alongside a 63% increase in forestry activity (Fig. 4D). This may reflect inconsistencies in how protection status is defined across jurisdictions, with some areas allowing logging still classified as strictly protected (*43, 47*).

Discussion

A recent study using structure-focused metrics suggested that 75% of the world's forests are becoming less fragmented as patch counts decline with forest loss (*7*) (Fig. 1F). While this conclusion is mathematically valid, our analysis incorporating connectivity and aggregation reveals the opposite: most forests, especially in the tropics, have become more fragmented over the past two decades. These findings align with prior studies showing increasing fragmentation in the tropics, with declining cover, more edge habitats, and reduced core areas (*34-36*). This trend holds across varying forest cover thresholds used to define forest grid cells (Fig. S17) and is primarily driven by declining connectivity and aggregation.

The divergences among fragmentation metrics highlight the importance of assessing not only forest areas but also the spatial arrangement of patches to evaluate changes in landscape integrity (*11, 12*). Structure-focused metrics, such as the SFI, capture a distinct and meaningful dimension of fragmentation related to patch size, number, and edge complexity (Fig. 2A). They are especially valuable for isolating fragmentation *per se* from habitat loss (*11, 17-19*), and for comparing sites with similar forest cover but differing patch structures (*13*). However, they reflect only one of three critical axes–structure, aggregation, and connectivity (Fig. 2A)–and can yield misleading results when forest cover changes alongside fragmentation, whether over time or across space. For example, they may indicate reduced fragmentation when patch numbers decline, even as habitat loss degrades connectivity and ecosystem function (Fig. 1C).

In contrast, connectivity- and aggregation-focused metrics offer a more ecologically meaningful perspective for detecting and interpreting fragmentation over time. They show stronger alignment with key ecological indicators such as metapopulation capacity and net primary productivity (Fig. S10), and directly reflect functional landscape properties that affect biodiversity persistence (*25, 31*). Notably, the strong correlation between the CFI and metapopulation capacity suggests that the CFI offers a computationally efficient proxy for ecological connectivity.

These differences among fragmentation metrics underscore the need for ecologically meaningful indicators in conservation planning (*11, 19*). For instance, both the CFI and AFI detect increased fragmentation across pantropical regions, consistent with high deforestation rates (*42*), and reveal 82% and 79% lower fragmentation in strictly protected areas compared to matched non-protected ones, respectively (Fig. 4A, S18). These reductions were largely driven by declines in agricultural activity (Fig. 4B). In contrast, the SFI suggests declining fragmentation both within and outside tropical protected areas (Fig. S18), illustrating how reliance on structure-based metrics alone can obscure ecological degradation and potentially mislead conservation efforts. To fully evaluate forest fragmentation and its ecological

consequences, all three dimensions—structure, aggregation, and connectivity—must be considered in tandem. However, metrics that capture connectivity and aggregation offer greater ecological relevance for understanding functional landscape change and guiding effective conservation.

Given the ecological relevance of connectivity-focused metrics, we used the CFI to assess the primary drivers of fragmentation and the effectiveness of protected areas across forest biomes. Our analysis shows that permanent forest conversion accounts for only 15% of global connectivity-focused fragmentation, while wildfires—intensified by climate change—contribute another 14% (Fig. 3). The remaining 71% was primarily driven by agricultural and forestry activities that can often represent temporary transitions, highlighting opportunities for restoration (*3, 8*). Protected areas mitigate these impacts, though their effectiveness varies by biome. Tropical forests benefit most, with reduced fragmentation primarily due to lower agricultural encroachment. By contrast, temperate and boreal forests show slight increases in fragmentation within protected areas, mainly driven by ongoing forestry. These patterns underscore the need for biome-specific conservation strategies that reflect distinct regional pressures.

While our study provides important insights into global forest fragmentation and its ecological implications, several limitations may affect the accuracy of our estimates. Landsat-derived data likely underestimates fragmentation by failing to detect narrow barriers, such as roads less than 30 meters wide (*48, 49*). Additionally, this forest cover product does not distinguish between natural forests and agroforestry, potentially underestimating natural forest loss (*37*). Conversely, using a 5-meter height threshold to define forests may not fully capture restoration trends, as degraded forests with slow regrowth below this height remain undetected (*37*).

In conclusion, our study reveals widespread declines in forest ecological integrity over the past two decades, driven largely by human activity. The stark divergence among fragmentation metrics underscore the urgent need for ecologically relevant tools to accurately assess and address these changes. As human pressures on nature intensify, such tools will be essential for guiding effective conservation and reversing global trends in fragmentation and biodiversity loss.

References

1. G. B. Bonan, Forests and Climate Change: Forcings, Feedbacks, and the Climate Benefits of Forests. *Science* **320**, 1444 (2008).
2. Y. Pan *et al.*, A Large and Persistent Carbon Sink in the World's Forests. *Science* **333**, 988-993 (2011).
3. L. Mo *et al.*, Integrated global assessment of the natural forest carbon potential. *Nature* **624**, 92-101 (2023).
4. H. Ma *et al.*, The global biogeography of tree leaf form and habit. *Nature Plants* **9**, 1795-1809 (2023).
5. Y. Zou *et al.*, Positive feedbacks and alternative stable states in forest leaf types. *Nature Communications* **15**, 4658 (2024).
6. Z. Wu *et al.*, Poleward shifts in the maximum of spring phenological responsiveness of Ginkgo biloba to temperature in China. *New Phytologist* **240**, 1421-1432 (2023).
7. J. Ma, J. Li, W. Wu, J. Liu, Global forest fragmentation change from 2000 to 2020. *Nature Communications* **14**, 3752 (2023).
8. P. G. Curtis, C. M. Slay, N. L. Harris, A. Tyukavina, M. C. Hansen, Classifying drivers of global forest loss. *Science* **361**, 1108-1111 (2018).
9. W. F. Laurance, G. B. Williamson, Positive Feedbacks among Forest Fragmentation, Drought, and Climate Change in the Amazon. *Conserv Biol* **15**, 1529-1535 (2001).
10. A. C. Staver, S. Archibald, S. Levin, The global extent and determinants of savanna and forest as

alternative biome states. *Science* **334**, 230-232 (2011).
11. N. M. Haddad *et al.*, Habitat fragmentation and its lasting impact on Earth's ecosystems. *Science Advances* **1**, e1500052.
12. M. Pfeifer *et al.*, Creation of forest edges has a global impact on forest vertebrates. *Nature* **551**, 187-191 (2017).
13. T. Gonçalves-Souza *et al.*, Species turnover does not rescue biodiversity in fragmented landscapes. *Nature*, (2025).
14. CBD, "Aichi Target 11," (2010).
15. B. IPBES. (Bonn Germany, 2019), pp. 1148.
16. L. Fahrig, Effects of Habitat Fragmentation on Biodiversity. *Annual Review of Ecology, Evolution, and Systematics* **34**, 487-515 (2003).
17. L. Fahrig, Habitat fragmentation: A long and tangled tale. *Global Ecol Biogeogr* **28**, 33-41 (2019).
18. L. Fahrig *et al.*, Is habitat fragmentation bad for biodiversity? *Biological Conservation* **230**, 179-186 (2019).
19. R. J. Fletcher *et al.*, Is habitat fragmentation good for biodiversity? *Biological Conservation* **226**, 9-15 (2018).
20. A. E. Martin, L. Fahrig, Habitat specialist birds disperse farther and are more migratory than habitat generalist birds. *Ecology* **99**, 2058-2066 (2018).
21. F. Riva, L. Fahrig, The disproportionately high value of small patches for biodiversity conservation. *Conservation Letters* **15**, e12881 (2022).
22. J. Rybicki, N. Abrego, O. Ovaskainen, Habitat fragmentation and species diversity in competitive communities. *Ecol Lett* **23**, 506-517 (2020).
23. J. N. G. Willmer, T. Püttker, J. A. Prevedello, Global impacts of edge effects on species richness. *Biological Conservation* **272**, 109654 (2022).
24. J. Oehri, S. L. R. Wood, E. Touratier, B. Leung, A. Gonzalez, Rapid evaluation of habitat connectivity change to safeguard multispecies persistence in human-transformed landscapes. *Biodiversity and Conservation* **33**, 4043-4071 (2024).
25. I. Hanski *et al.*, Ecological and genetic basis of metapopulation persistence of the Glanville fritillary butterfly in fragmented landscapes. *Nature Communications* **8**, 14504 (2017).
26. M. Beger *et al.*, Demystifying ecological connectivity for actionable spatial conservation planning. *Trends Ecol Evol* **37**, 1079-1091 (2022).
27. K. S. McGarigal, S. Cushman, M. Neel, E. Ene, FRAGSTATS: Spatial pattern analysis program for categorical maps. (2002).
28. N. H. Schumaker, Using Landscape Indices to Predict Habitat Connectivity. *Ecology* **77**, 1210-1225 (1996).
29. J. A. G. Jaeger, Landscape division, splitting index, and effective mesh size: new measures of landscape fragmentation. *Landscape Ecol* **15**, 115-130 (2000).
30. H. S. He, B. E. DeZonia, D. J. Mladenoff, An aggregation index (AI) to quantify spatial patterns of landscapes. *Landscape Ecol* **15**, 591-601 (2000).
31. I. Hanski, O. Ovaskainen, The metapopulation capacity of a fragmented landscape. *Nature* **404**, 755-758 (2000).
32. D. R. Patton, A Diversity Index for Quantifying Habitat "Edge". *Wildlife Society Bulletin (1973-2006)* **3**, 171-173 (1975).
33. H. Li, J. Wu, Use and misuse of landscape indices. *Landscape Ecol* **19**, 389-399 (2004).
34. F. Taubert *et al.*, Global patterns of tropical forest fragmentation. *Nature* **554**, 519-522 (2018).
35. M. C. Hansen *et al.*, The fate of tropical forest fragments. *Science Advances* **6**, eaax8574.

36. R. Fischer *et al.*, Accelerated forest fragmentation leads to critical increase in tropical forest edge area. *Science Advances* **7**, eabg7012.
37. P. Potapov *et al.*, The Global 2000-2020 Land Cover and Land Use Change Dataset Derived From the Landsat Archive: First Results. *Frontiers in Remote Sensing* **3**, (2022).
38. L. Tischendorf, Can landscape indices predict ecological processes consistently? *Landscape Ecol* **16**, 235-254 (2001).
39. L. Tischendorf, L. Fahrig, On the usage and measurement of landscape connectivity. *Oikos* **90**, 7-19 (2000).
40. UNEP-WCMC and IUCN (2023), Protected Planet: The World Database on Protected Areas (WDPA) [On-line], [09/2023], Cambridge, UK: UNEP-WCMC and IUCN Available at: www.protectedplanet.net.
41. E. Dinerstein *et al.*, An Ecoregion-Based Approach to Protecting Half the Terrestrial Realm. *Bioscience* **67**, 534-545 (2017).
42. J. S. Sze, L. R. Carrasco, D. Childs, D. P. Edwards, Reduced deforestation and degradation in Indigenous Lands pan-tropically. *Nat Sustain* **5**, 123-130 (2022).
43. J. Geldmann, A. Manica, N. D. Burgess, L. Coad, A. Balmford, A global-level assessment of the effectiveness of protected areas at resisting anthropogenic pressures. *Proceedings of the National Academy of Sciences* **116**, 23209-23215 (2019).
44. P. J. Ferraro, M. M. Hanauer, K. R. E. Sims, Conditions associated with protected area success in conservation and poverty reduction. *Proceedings of the National Academy of Sciences* **108**, 13913-13918 (2011).
45. V. Graham *et al.*, Southeast Asian protected areas are effective in conserving forest cover and forest carbon stocks compared to unprotected areas. *Scientific Reports* **11**, 23760 (2021).
46. P. J. Negret *et al.*, Effects of spatial autocorrelation and sampling design on estimates of protected area effectiveness. *Conserv Biol* **34**, 1452-1462 (2020).
47. J. Geldmann *et al.*, Changes in protected area management effectiveness over time: A global analysis. *Biological Conservation* **191**, 692-699 (2015).
48. B. Slagter *et al.*, Monitoring road development in Congo Basin forests with multi-sensor satellite imagery and deep learning. *Remote Sensing of Environment* **315**, 114380 (2024).
49. J. E. Engert *et al.*, Ghost roads and the destruction of Asia-Pacific tropical forests. *Nature* **629**, 370-375 (2024).
50. Y. Zou, "Yibiaozou/Global_ForestFRAG: Global fragmentation trends during 2000-2020". Zenodo, Feb. 17, 2025. doi: 10.5281/zenodo.14883322.
51. Y. Zou, "Global fragmentation trends during 2000-2020". Zenodo, June 20, 2025. doi: 10.5281/zenodo.15703795.
52. M. H. K. Hesselbarth, M. Sciaini, K. A. With, K. Wiegand, J. Nowosad, landscapemetrics: an open-source R tool to calculate landscape metrics. *Ecography* **42**, 1648-1657 (2019).
53. I. Hanski, A Practical Model of Metapopulation Dynamics. *J Anim Ecol* **63**, 151-162 (1994).
54. R. Levins, Some Demographic and Genetic Consequences of Environmental Heterogeneity for Biological Control1. *Bulletin of the Entomological Society of America* **15**, 237-240 (1969).
55. J. K. Schnell, G. M. Harris, S. L. Pimm, G. J. Russell, Estimating extinction risk with metapopulation models of large-scale fragmentation. *Conserv Biol* **27**, 520-530 (2013).
56. R. Huang, S. L. Pimm, C. Giri, Using metapopulation theory for practical conservation of mangrove endemic birds. *Conserv Biol* **34**, 266-275 (2020).
57. M. Strimas-Mackey, J. F. Brodie, Reserve design to optimize the long-term persistence of multiple species. *Ecol Appl* **28**, 1354-1361 (2018).

58. C. H. Albert, B. Rayfield, M. Dumitru, A. Gonzalez, Applying network theory to prioritize multispecies habitat networks that are robust to climate and land-use change. *Conserv Biol* **31**, 1383-1396 (2017).
59. H. Mu *et al.*, A global record of annual terrestrial Human Footprint dataset from 2000 to 2018. *Scientific Data* **9**, 176 (2022).
60. A. Thomas *et al.*, Fragmentation and thresholds in hydrological flow-based ecosystem services. *Ecological Applications* **30**, e02046 (2020).
61. D. M. Olson *et al.*, Terrestrial Ecoregions of the World: A New Map of Life on Earth: A new global map of terrestrial ecoregions provides an innovative tool for conserving biodiversity. *Bioscience* **51**, 933-938 (2001).
62. J. Mattisson *et al.*, Home range size variation in a recovering wolf population: evaluating the effect of environmental, demographic, and social factors. *Oecologia* **173**, 813-825 (2013).
63. H. Zhao *et al.*, Individual-level performance of nature reserves in forest protection and the effects of management level and establishment age. *Biological Conservation* **233**, 23-30 (2019).
64. D. N. Karger, D. R. Schmatz, G. Dettling, N. E. Zimmermann, High-resolution monthly precipitation and temperature time series from 2006 to 2100. *Scientific Data* **7**, 248 (2020).
65. C. T. Lloyd *et al.*, Global spatio-temporally harmonised datasets for producing high-resolution gridded population distribution datasets. *Big Earth Data* **3**, 108-139 (2019).
66. J. Lizundia-Loiola, G. Otón, R. Ramo, E. Chuvieco, A spatio-temporal active-fire clustering approach for global burned area mapping at 250 m from MODIS data. *Remote Sensing of Environment* **236**, 111493 (2020).
67. D. J. Weiss *et al.*, A global map of travel time to cities to assess inequalities in accessibility in 2015. *Nature* **553**, 333-336 (2018).
68. J. Schleicher *et al.*, Statistical matching for conservation science. *Conserv Biol* **34**, 538-549 (2020).
69. L. G. S. Ribas, R. L. Pressey, L. M. Bini, Estimating counterfactuals for evaluation of ecological and conservation impact: an introduction to matching methods. *Biological Reviews* **96**, 1186-1204 (2021).
70. J. Schleicher, C. A. Peres, T. Amano, W. Llactayo, N. Leader-Williams, Conservation performance of different conservation governance regimes in the Peruvian Amazon. *Scientific Reports* **7**, 11318 (2017).
71. C. F. Dormann *et al.*, Collinearity: a review of methods to deal with it and a simulation study evaluating their performance. *Ecography* **36**, 27-46 (2013).
72. D. Ho, K. Imai, G. King, E. A. Stuart, MatchIt: Nonparametric Preprocessing for Parametric Causal Inference. *Journal of Statistical Software* **42**, 1 - 28 (2011).
73. A. Blackman, A. Pfaff, J. Robalino, Paper park performance: Mexico's natural protected areas in the 1990s. *Global Environmental Change* **31**, 50-61 (2015).
74. A. Olmos, P. Govindasamy, Propensity Scores: A Practical Introduction Using R. *Journal of MultiDisciplinary Evaluation* **11**, 68-88 (2015).
75. W. H. Kruskal, W. A. and Wallis, Use of Ranks in One-Criterion Variance Analysis. *Journal of the American Statistical Association* **47**, 583-621 (1952).
76. S. Running, Zhao, M., in *MODIS/Terra Net Primary Production Gap-Filled Yearly L4 Global 500m SIN Grid V061 [Data set]*. (NASA EOSDIS Land Processes Distributed Active Archive Center, 2021).

Acknowledgments: We warmly thank all the members of the Crowther lab team, including those not listed as coauthors of the study, for their incredible support.

Funding: This work was supported by grants to CMZ from the Ambizione Fellowship program (#PZ00P3_193646), TWC from Bernina Foundation and DOB Ecology, GRS from the Ambizione Fellowship program (#PZ00P3_216194) and KAG from Marie Skłodowska-Curie Actions Postdoctoral Fellowship (EP/Z000831/1).

Author contributions: YZ, CMZ and TWC conceived, developed and wrote the paper. YZ performed the analyses. All authors reviewed and provided input on the manuscript.

Competing interests: Authors declare that they have no competing interests.

Data and materials availability: All data used in this study are from open-source databases and referenced in the paper. Code is available in https://github.com/Yibiaozou/Global_ForestFRAG and Zenodo (*50*). Major dataset and outcome maps of fragmentation metrics are also available in Zenodo (*51*).

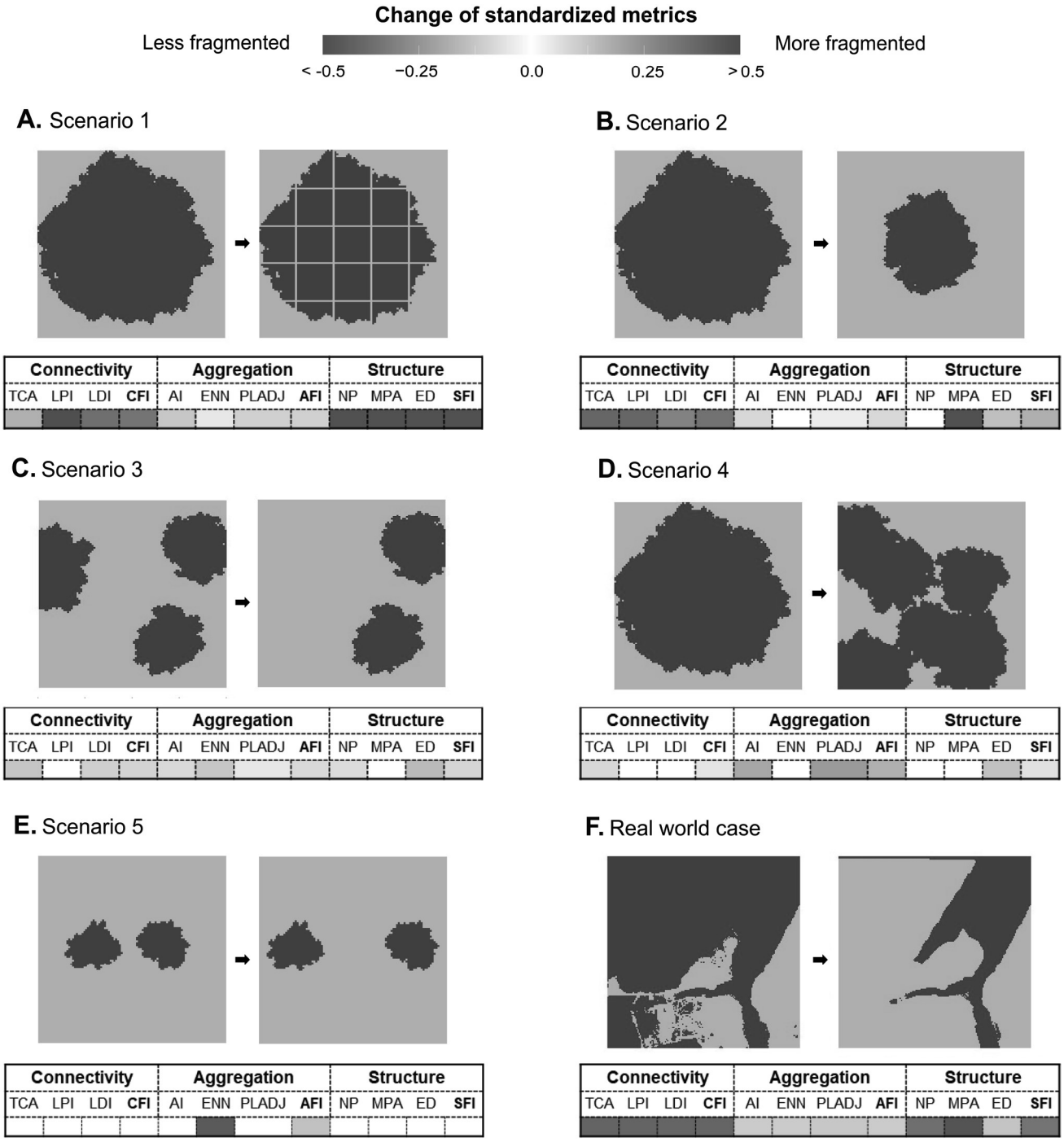

420 **Fig. 1 | Responses of fragmentation metrics to simulated (A-E) and observed (F) landscape change scenarios. A**, Transition from a single forest patch with 60% canopy cover to multiple smaller patches with minimal cover loss. **B**, Reduction of a single forest patch from 60% to 20% cover. **C**, Removal of one of three equally-sized forest patches. **D**, Transformation of a circular patch with 60% cover into an irregular shape with the same coverage but a longer perimeter. **E**, Increased distance between two previously proximate patches. **F**, Observed deforestation in an Amazon forest site 425 from 2000 (left, 72% cover) to 2020 (right, 26% cover); similar patterns occur in other sites (Fig. S2). Our analysis shows that scenarios 2 and 3 are the most prevalent globally, affecting 18% and 46% of forests experiencing cover loss, respectively (Fig. S3). While scenarios 4 and 5 are hypothetical and may not frequently occur in real forested landscapes, they help illustrate how aggregation-focused metrics respond to changes in patch shape and distance compared to connectivity- and structure-focused metrics. For each scenario, changes were assessed using 12 normalized fragmentation

metrics (scaled from 0 to 1, see Tables 1 and S1 for details), categorized into three groups: connectivity-focused, aggregation-focused and structure-focused metrics. Positive values indicate increased fragmentation. Red signifies a fragmentation increase, blue indicates a decrease, and white indicates no change, with darker shades representing greater magnitude. The CFI, AFI, and SFI, representing integrated indices for connectivity, aggregation, and structure, are highlighted in bold.

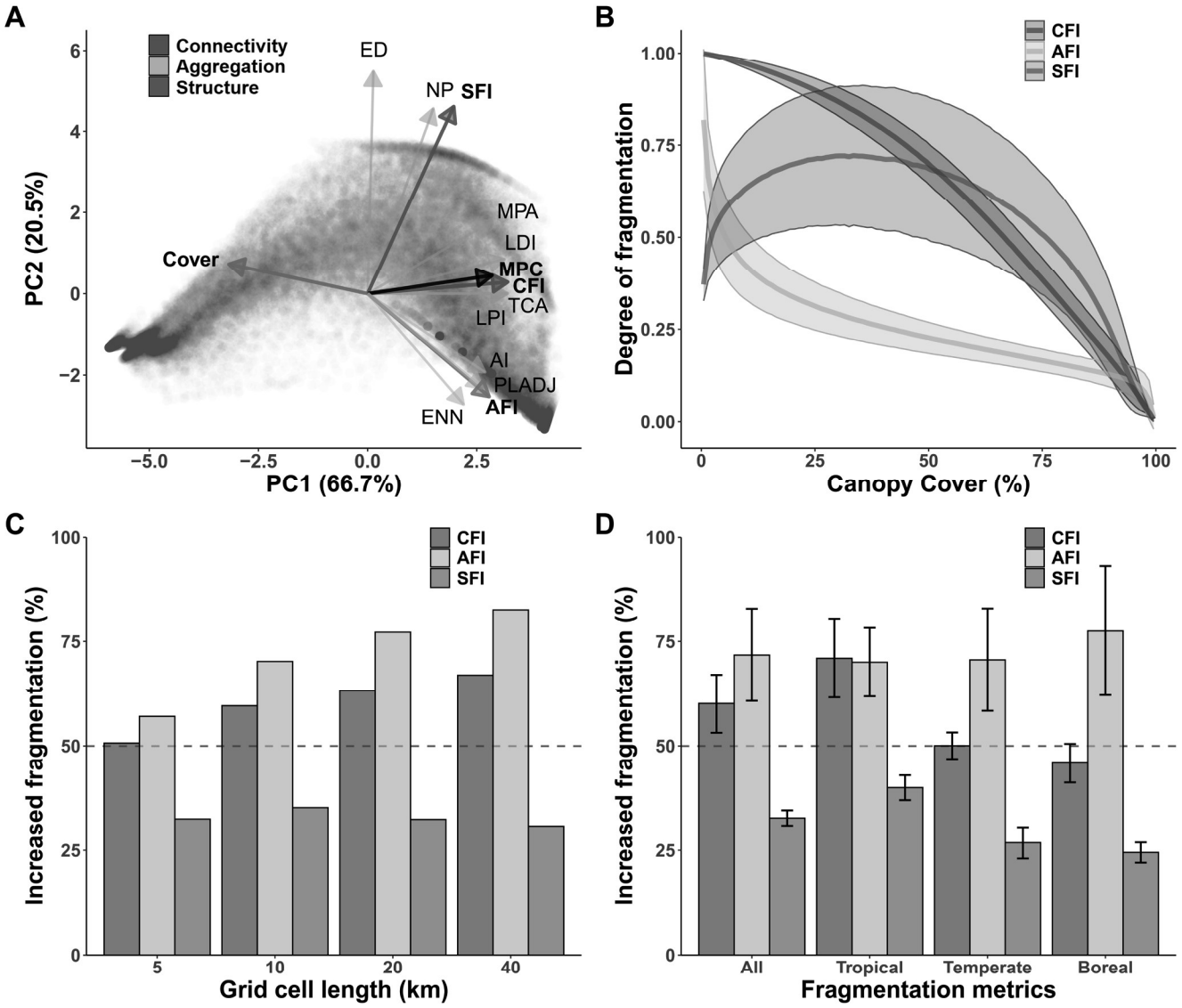

Fig. 2 | Classification and analysis of fragmentation metrics. A, The major axes of forest fragmentation: Principal Component Analysis (PCA) Biplot showing the distribution of various fragmentation metrics applied to a 10% random sample of all grid cells (forest cover > 0) for the year 2000. Metrics are color-coded based on their focus: connectivity-focused in red, aggregation-focused in orange, and structure-focused in blue. The integrated indices—Connectivity-based Fragmentation Index (CFI), Aggregation-based Fragmentation Index (AFI), and Structure-based Fragmentation Index (SFI, formerly termed FFI from Ma et al., (2023))—are highlighted in darker shades within their groups. Forest cover (in dark cyan) is also included. A Pair-wise Multivariate Analysis of Variance (MANOVA) confirms significant differences among loadings of these three groups ($p < 0.001$), indicating distinct clustering. The Metapopulation Capacity (MPC; depicted in black), a critical metric for functional connectivity, aligns closely with connectivity-focused metrics. See Fig. S3 for PCA biplots on the 12 fragmentation metrics across all grid cells in both years 2000 and 2020. **B**, Relationship between the observed fragmentation degree (based on the CFI, AFI and SFI) and canopy cover for all analyzed forest

grid cells in the year 2000. Solid lines represent mean fragmentation values, the shaded areas represent mean ± std. **C**, Proportion of global forest grid cell areas with increased fragmentation between 2000 and 2020 at different grid cell scales, based on the CFI, AFI and SFI. **D**, Proportion of forest grid cell areas with increased fragmentation (mean ± std, over different grid cell scales) between 2000 and 2020 across global forest grid cells and in different forest biomes, based on the CFI, AFI and SFI. Panels C and D include only forest grid cells with forest cover >30% in 2000. Results remained consistent across different forest cover thresholds used to define forest grid cells (Fig. S17).

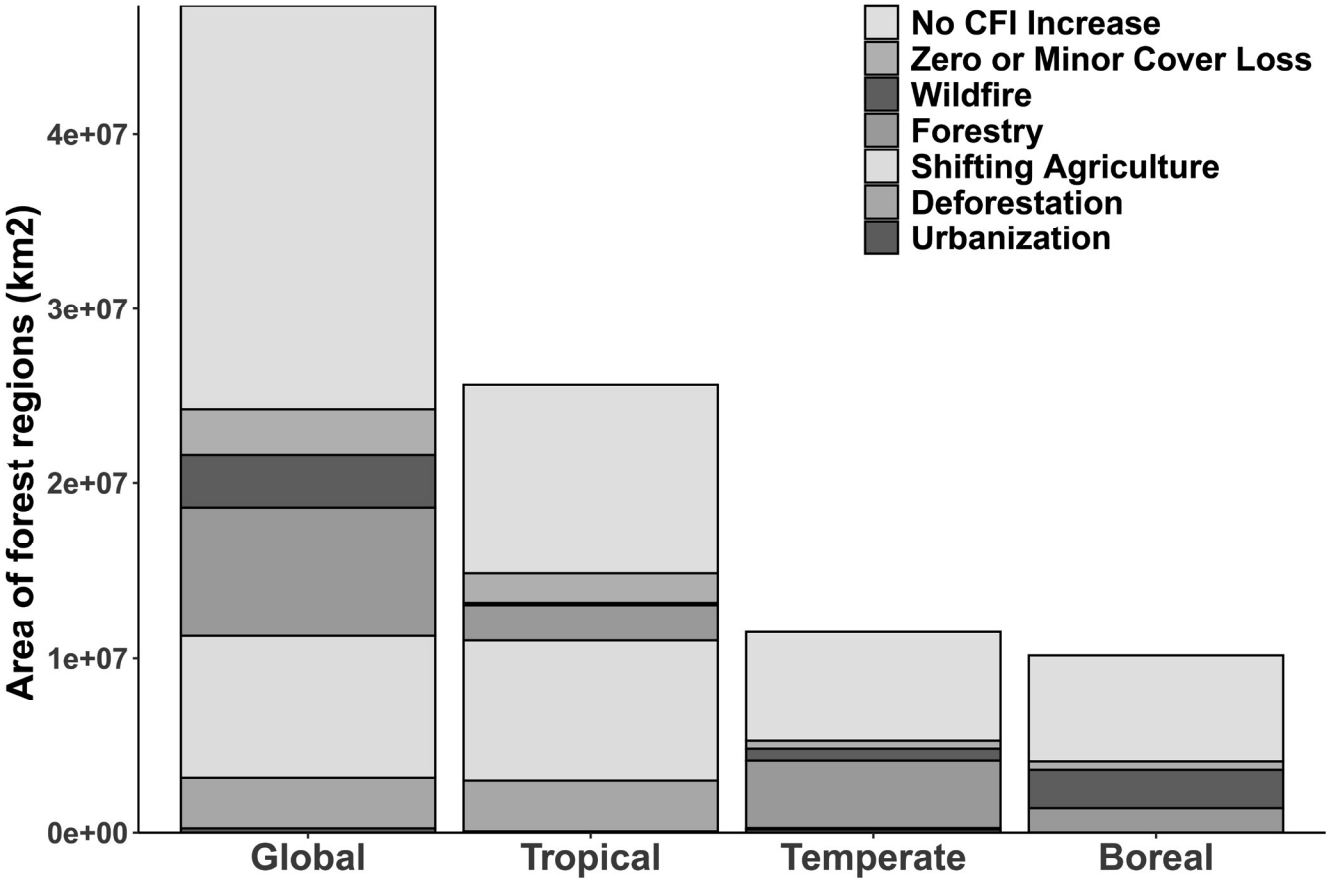

Fig. 3. Drivers of forest fragmentation trends (2000–2020) across biomes. Total area of forest regions (grid cells with >30% canopy cover at 2.5 arc-min [~5 km] resolution, the finest resolution available) affected by different fragmentation drivers at global and biome scales. “No CFI increase” represents forest regions where fragmentation levels have remained stable or decreased. "Zero or minor cover loss" includes areas where fragmentation slightly increased due to unknow cause but with minor or no forest cover loss. All other categories represent regions with increased fragmentation driven by specific factors, including i) “Wildfire”, where forest burning occurred without subsequent human conversion or agricultural activity, ii) “Forestry”, representing large-scale harvesting within managed forests with signs of regrowth, iii) “Shifting agriculture”, referring to small- to medium-scale forest conversion for agriculture, later abandoned and followed by forest regrowth, iv) “Deforestation”, characterized by permanent forest loss due to commodity-driven activities such as agriculture, mining, or energy infrastructure, and v) “Urbanization”, where forests have been converted for urban expansion. The drivers are arranged from “Wildfire” (top) to “Urbanization” (bottom) to reflect the increasing degree of irreversible forest loss.

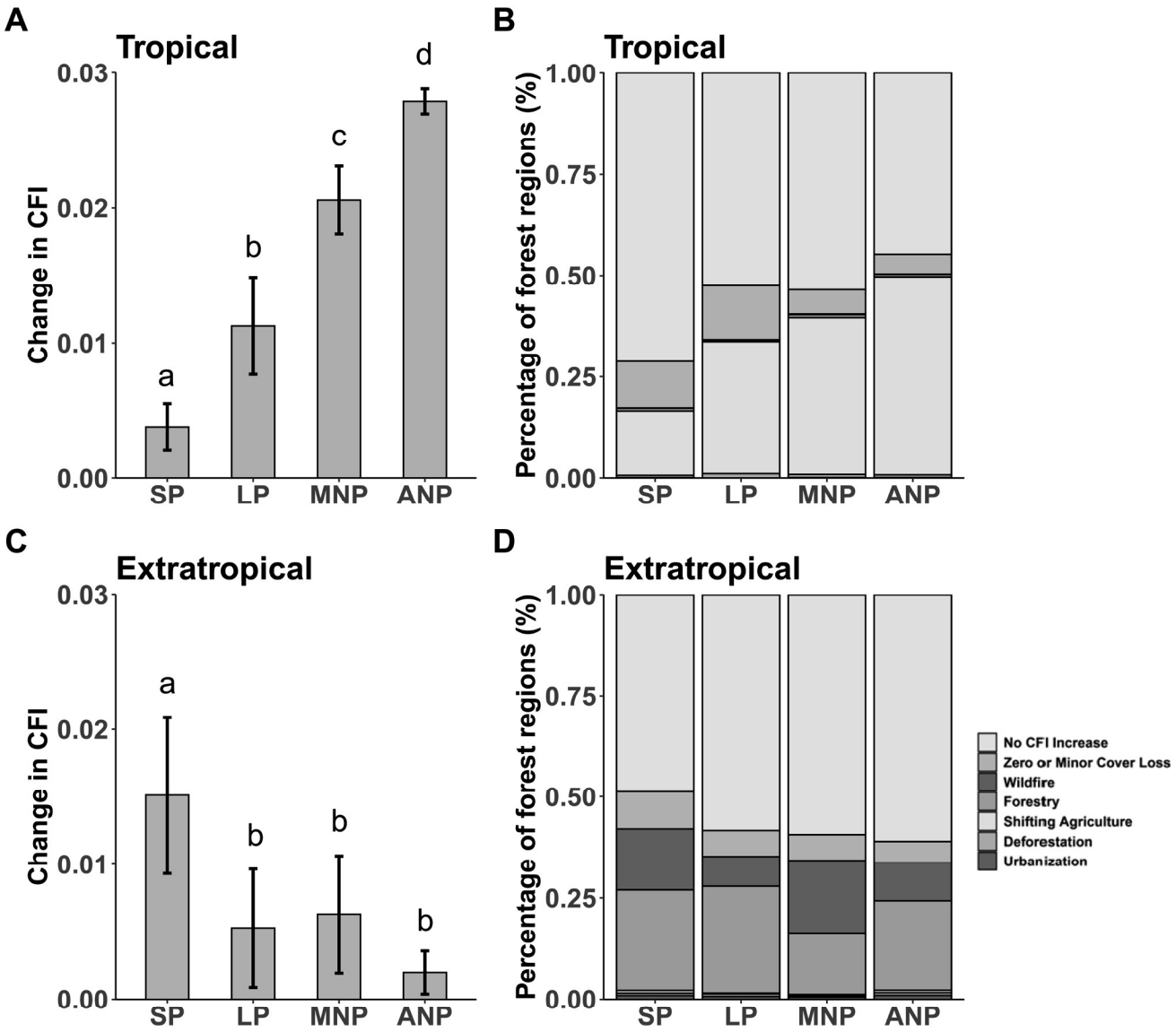

Fig. 4. Forest fragmentation trends (2000–2020) inside and outside protected areas. A and **C,** Changes in the degree of fragmentation (indicated by the CFI, mean ± 3 se) across forest grid cells (at 2.5 arc-min [~5 km] resolution) in strictly protected areas, loosely protected areas, matched non-protected areas, and all non-protected areas in tropical (**A**) and extratropical (**C**) forests. Kruskal-Wallis and post-hoc Mann-Whitney U tests (Table S4-5) show that in tropical forests (**A**), fragmentation levels significantly differ across all protection categories ($p < 0.001$), while in extratropical forests (**C**), only the "Strictly Protected" group is significantly different from all other groups ($p < 0.05$). **B** and **D**, Proportions of forest regions experiencing fragmentation due to different drivers across different protection categories in tropical (**B**) and extratropical (**D**) regions. "No CFI increase" represents areas where fragmentation levels have remained stable or decreased. "Zero or minor cover loss" includes areas where fragmentation slightly increased due to unknow cause but with minor or no forest cover loss. All other categories represent regions with increased fragmentation driven by specific factors such as forestry, shifting agriculture, deforestation, or urbanization. To address spatial autocorrelation, we only

included forest grid cells at least 40 km apart.

495

Table 1. Overview of landscape-level fragmentation metrics.

	Metric	Full name	Description	Reference
	Canopy cover	**Forest cover percentage**	The percentage of the landscape covered by forests.	McGarigal et al. (2002) (*27*)
Connectivity-focused	TCA	Total core area	The sum of core areas of all patches belonging to forests. A cell is defined as core area if all of its neighboring cells are forests.	McGarigal et al. (2002) (*27*)
	LPI	Largest patch index	The percentage of the landscape covered by the corresponding largest patch of forest.	McGarigal et al. (2002) (*27*)
	LDI	Landscape division index	The probability that two randomly selected cells are not located in the same patch of forest.	Jaeger (2000) (*29*)
	CFI	**Connectivity-based fragmentation index**	Synthetic metric integrating TCA, LPI and LDI.	This paper
Aggregation-focused	AI	Aggregation index	The number of like adjacencies divided by the theoretical maximum possible number of like adjacencies for forest cells.	He et al. (2000) (*30*)
	PLADJ	Percentage of Like Adjacencies	The number of adjacencies between forest cells divided by the number of adjacencies between forest and non-forests cells.	McGarigal et al. (2002) (*27*)
	ENN	Mean of Euclidean nearest-neighbor distance	The mean Euclidean distance to the nearest neighboring patch for each forest patch.	McGarigal et al. (2002) (*27*)
	AFI	**Aggregation-based fragmentation index**	Synthetic metric integrating AI, PLADJI and ENN.	This paper
Structure-focused	NP	Number of patches	Number of distinct forest patches.	McGarigal et al. (2002) (*27*)
	MPA	Mean patch area	The mean of all patch areas belonging to forests.	McGarigal et al. (2002) (*27*)
	ED	Edge density	The length sum of all edges of forest divided by the landscape area (In our study the landscape area is the grid cell area).	McGarigal et al. (2002) (*27*)
	SFI	**Structure-based fragmentation index**	Synthetic metric integrating NP, MPA and ED. This index was called FFI in Ma et al. (2023).	Ma et al. (2023) (*7*)
Functional connectivity	**MPC**	**Metapopulation capacity**	A relative measure of the ability of a spatially explicit landscape to support long-term species persistence based on connectivity and area of habitat.	Hanski & Ovaskainen (2000) (*31*)

Science
AAAS

Supplementary Materials for

Forest fragmentation increased in over half of global forests from 2000 to 2020

Yibiao Zou[1*], Thomas W. Crowther[1,2], Gabriel Reuben Smith[1], Haozhi Ma[3], Lidong Mo[1], Lalasia Bialic-Murphy[1], Peter Potapov[4], Klementyna A. Gawecka[5,9], Chi Xu[5], Pablo J. Negret[7,10], Thomas Lauber[1], Zhaofei Wu[1,3,8], Dominic Rebindaine[1], Constantin M. Zohner[1]
Corresponding author: yibiao.zou@usys.ethz.ch

The PDF file includes:

Materials and Methods

Data processing

High-resolution (30 m) global tree cover data for 2000 and 2020 were sourced from the Global Land Cover and Land Use (GLCLU) dataset (*37*). Pixels with tree heights ≥ 5 m, as per the Landsat pixel scale (30 m resolution), were identified as forest pixels, aligning with the FAO definition (*37*). These data were processed into binary forest maps for both years and subdivided into 5807257 grid cells with a resolution of 2.5 arc-minutes (~ 5 km in the equator) in geographic coordinates (EPSG: 4326). Within these cells, twelve fragmentation-related landscape metrics (see Tables 1 and S1) were computed using the "landscapemetric" R package (*52*).

Standardization of fragmentation metrics

We compiled a set of nine widely-used fragmentation metrics from previous studies (*7, 27-32*) (see Table S1 for details). These metrics include:

- Mean Patch Area (MPA): Average size of individual patches.
- Edge Density (ED): Total edge length per unit area.
- Number of Patches (NP): Total count of forest patches.
- Total Core Area (TCA): Total area of core forest patches.
- Largest Patch Index (LPI): Percentage of the landscape occupied by the largest patch.
- Landscape Division Index (LDI): Probability that two randomly placed points fall in different patches.
- Aggregation Index (AI): Degree of patch aggregation.
- Percentage of Like Adjacencies (PLADJ): Measures patch connectivity based on patch-to-edge length adjacency.
- Mean of Euclidean Nearest Neighbor distance (ENN): Average distance between patches.

These metrics were computed for each grid cell with forest cover > 0% across the entire dataset for the years 2000 and 2020, using the "landscapemetric" R package (*52*). To facilitate interpretation, we classified these metrics into three broad categories: The nine fragmentation metrics can be broadly classified into three classes:

1. Structure-focused metrics (NP, ED, MPA) capture changes in patch structure but are less sensitive to the total habitat area.
2. Connectivity-focused metrics (TCA, LPI, LDI) assess the extent and spatial arrangement of core forest areas. LDI specifically measures the probability that two randomly placed individuals reside within the same contiguous forest patch.
3. Aggregation-focused metrics (AI, PLADJ, ENN) characterize spatial clustering and edge-to-core relationships, reflecting landscape aggregation patterns.

This classification allows for a nuanced interpretation of fragmentation dynamics, distinguishing between changes in patch isolation, connectivity, and spatial clustering.

Given that the remote sensing tree cover product used in this study has a resolution of 30 m (*37*), forest patches were considered separate if their edge-to-edge nearest distance was ≥ 30 m, and the minimum patch size was set to 900 m^2 (equivalent to one pixel). To ensure consistency and comparability, we applied the same normalization procedure as in Ma et al. (2023). Specifically, we determined the upper and lower limit values of each fragmentation metric in 2020 using the following formulas:

$$Q_{upper} = Q_3 + 1.5 \times IQR \quad (1)$$

$$Q_{lower} = Q_1 - 1.5 \times IQR \quad (2)$$

where Q_{upper} and Q_{lower} represent the upper and lower limit values for each metric, respectively; Q_1 is the 25th percentile (lower quartile); Q_3 is the 75th percentile (upper quartile) of each landscape pattern metric; and IQR denotes the difference between Q_3 and Q_1. This method captures the distribution of the data in a realistic and intuitive manner, considering that landscape pattern metrics typically do not follow a normal distribution. We set pixel values exceeding the upper and lower limits to their corresponding limit values to mitigate the influence of extreme outliers.

To allow direct comparisons between the two study years, we applied the upper and lower limit values established for 2020 as a standard reference, and processed the 2000 data using the same approach. The normalization process was carried out using the following equation:

$$Y_{nor} = \begin{cases} \dfrac{X - X_{min}}{X_{max} - X_{min}}, & if\ X\ increases\ with\ fragmentation \\ 1 - \dfrac{X - X_{min}}{X_{max} - X_{min}}, & if\ X\ decreases\ with\ fragmentation \end{cases} \quad (3)$$

where Y_{nor} represents the normalized values for each of the nine fragmentation metrics, with values ranging from 0-1, where higher values indicate higher levels of fragmentation; X is the original value of each fragmentation metric; and X_{max} and X_{min} are the corresponding maximum and minimum values for that year.

In the next step, we derived integrated metrics for each of the three fragmentation classes: Structure-based Fragmentation Index (SFI), Connectivity-based Fragmentation Index (CFI), and Aggregation-based Fragmentation Index (AFI). These indices

were computed by aggregating the normalized values of the three individual metrics within each class using the following equations:

$$SFI = \frac{ED_{nor} + NP_{nor} + MPA_{nor}}{3} \quad (4)$$

$$CFI = \frac{LDI_{nor} + TCA_{nor} + LPI_{nor}}{3} \quad (5)$$

$$AFI = \frac{ENN_{nor} + PLADJ_{nor} + AI_{nor}}{3} \quad (6)$$

where ED_{nor}, NP_{nor}, MPA_{nor}, LDI_{nor}, TCA_{nor}, LPI_{nor}, ENN_{nor}, $PLADJ_{nor}$, ED_{nor}, NP_{nor}, MPA_{nor}, LDI_{nor}, TCA_{nor}, LPI_{nor}, ENN_{nor}, $PLADJ_{nor}$, and AI_{nor} represent the normalized values of the respective fragmentation metrics.

We then conducted a principal component analysis (PCA) to explore relationships among fragmentation metrics and assess their distinct contributions. The PCA was performed on a dataset containing the nine individual fragmentation metrics plus the three integrated indices (SFI, CFI, and AFI) for both the years 2000 and 2020 (Fig. S4A-B). The PCA results confirm that the three metric groups—structure, connectivity, and aggregation—form distinct and well-defined dimensions in the PCA space (Fig. 2A and S4), highlighting their unique contributions to understanding forest fragmentation. This classification helps disentangle different fragmentation patterns and improves the interpretability of fragmentation trends over time.

Metapopulation capacity

To determine which group of fragmentation metrics best represents connectivity, we calculated a well-developed and widely-used landscape-level connectivity metric, metapopulation capacity (MPC). Rooted in metapopulation theory (*31, 53, 54*), MPC quantifies the combined effects of habitat amount (Fig. S19) and configuration on species' metapopulation dynamics, which are driven by the processes of extinction and colonization of local populations within habitat patches. MPC is computed using the following equations:

$$MPC = \lambda_m$$
$$m_{ij} = \begin{cases} f(d_{ij}) a_j a_i^x, & i \neq j \\ a_j a_i^x, & i = j \end{cases} \quad (7)$$

where λ_m is the leading eigenvalue of a square 'landscape matrix' m, in which each element m_{ij} reflects connectivity between patches i and patch j as a function of patch attributes. These attributes include: patch area a_i and a_j in m^2, a dispersal probability function of interpatch distance $f(d_{ij})$, and an extinction probability constant x, commonly set to 0.5 (*24*). The dispersal probability function is modeled with a negative exponential kernel:

$$f(d_{ij}) = \exp(-\alpha d_{ij}) \quad (8)$$

where α is the inverse mean gap crossing distance and d_{ij} is the edge-to-edge Euclidean distance weighted by resistance between patches i and j in the habitat network.

For species-specific applications, α should be calibrated to species-specific traits. In our study, as we do not focus on specific species, we used a representative α value of 317 m, consistent with prior studies (*55, 56*), which represents the average dispersal distance for a wide range of terrestrial animals (*20, 55-58*). To model resistance, we used a global human footprint index map from the year 2000 (*59*). Due to the high computational cost, we calculated MPC for a 10% random subsample of forest grid cells within each forest type (tropical, temperate and boreal) for the year 2000. This process required several months to complete on the Euler Cluster at ETH Zurich.

To facilitate comparison with other metrics, we normalized MPC using equation (3) to ensure values range from 0 to 1 and increase with fragmentation. We then added the normalized MPC to the PCA biplot, which also included the 12 selected fragmentation metrics (Fig. 2A). The PCA biplot shows that connectivity-focused metrics (in red) are closely aligned with MPC, underscoring their ability to represent functional connectivity effectively.

Comparison of fragmentation metrics using landscape simulations

To evaluate the behavior of different fragmentation metrics under varying landscape configurations, we used the "landscapeR" R package (*60*) to create a series of 200,000 simulated landscapes. These landscapes varied in forest cover (from 0.1% to 100% in increments of 0.1%) and in the number of forest patches (from 1 to 200).

For each simulated landscape, we calculated the CFI, AFI and SFI, along with the other nine fragmentation metrics from which these integrated indices were derived. All 12 metrics were normalized to a range of 0-1, where higher values indicate higher levels of fragmentation.

To illustrate the behavior of these metrics, we selected five distinct landscape change scenarios that represent major types of fragmentation (Fig. 1):

(1) **Transition to multiple patches with retained coverage:** A single forest patch with 60% coverage transitions into tens of diverse patches while retaining the 60% coverage (Fig. 1A).
(2) **Forest shrinkage:** A forest patch with 60% coverage shrinks to 30% coverage (Fig. 1B).
(3) **Patch loss:** One of three equally-sized forest patches is removed (Fig. 1C).
(4) **Increased edge complexity:** Change from a circular forest patch with 60% coverage to a more irregularly shaped patch with longer edges but the same coverage (Fig. 1D).
(5) **Increased patch separation:** Two spatially proximate forest patches move further apart, increasing the inter-patch distance while maintaining the same coverage (Fig. 1E).

While scenarios (4) and (5) are hypothetical and may not fully reflect real-world landscapes, they provide valuable insights into how different metrics respond to specific fragmentation patterns.

Quantifying global fragmentation trends

To analyze global forest fragmentation trends, we first applied a filter to the raw dataset, retaining only forest grid cells with over 30% canopy cover in the year 2000. This resulted in a total of 3,233,983 grid cells at 2.5 arc-minute (5 km) resolution. For these cells, we calculated the differences in fragmentation metrics and forest cover between 2000 and 2020.

To quantify the sensitivity of different fragmentation metrics to forest cover changes, we performed simple linear regression to predict changes in each fragmentation metric as a function of forest cover change across forest grids within each ecoregion (*41*). The sensitivity of the metrics was quantified using the coefficients of determination (R^2) from these regressions.

For each of the 12 fragmentation metrics, we calculated the proportions of forest grid cell areas (corrected for latitudinal differences) that experienced increased fragmentation globally, as well as within tropical, temperate, and boreal forests (Fig. 2C-D). Biome classification followed the WWF system (*61*) (Fig. S21-22), with the following definitions:

- Tropical forests include "Tropical and Subtropical Moist Broadleaf Forests", "Tropical and Subtropical Dry Broadleaf Forests", "Tropical and Subtropical Coniferous Forests", and "Tropical and Subtropical Grasslands, Savannas, and Shrublands".
- Temperate forests include "Temperate Broadleaf and Mixed Forests", "Temperate Coniferous Forests", "Mediterranean Forests, Woodlands and Scrub".
- Boreal forests include "Boreal Forests/Taiga".

Detailed biome classifications are provided in Table S2.

Dependence on scale and forest cover thresholds

To investigate the scale-dependence of different fragmentation metrics, we replicated the above analysis using grid cell scales of 5, 10, and 20 arc-minutes, corresponding approximately to 10, 20, and 40 km at the equator (Fig. 2C-D). The largest scale, 40 km, was chosen because it encompasses the maximum home range (approximately 1600 km²) of large mammals with strong movement capabilities, such as wolves (*62*).

To explore the effects of canopy cover thresholds used to define forest grid cells, we replicated the analysis using cover thresholds of 10%, 20% and 40% (Fig. S17). The results remained consistent with those obtained using the 30% cover threshold (Fig. 2C-D).

Spatial visualization of fragmentation trajectories

To capture the spatial variation in fragmentation trends, we created maps of changes in fragmentation based on the CFI, AFI and SFI at 5 km resolution using geographic coordinates (EPSG: 4326) and the R package "raster". We categorized all forest grid cells into six distinct landscape-change scenarios based on their forest cover and fragmentation trajectories (Fig. S9):

(1) **No forest loss:** Grid cells with no forest cover loss during 2000-2020.
(2) **Increased fragmentation (all metrics):** Grid cells with decreased forest cover where CFI, AFI and SFI all indicate an increase in fragmentation.
(3) **Inconsistent SFI:** Grid cells with decreased forest cover where the CFI and AFI indicate increased fragmentation, but the SFI indicates a decrease.
(4) **Inconsistent AFI:** Grid cells with decreased forest cover where the CFI and SFI indicate increased fragmentation, but the AFI indicates a decrease.
(5) **CFI-only increase:** Grid cells with decreased forest cover where the CFI indicates increased fragmentation, but both the AFI and SFI indicate a decrease
(6) **CFI decrease**: Grids with decreased forest cover where the CFI indicates a decrease in fragmentation.

Our analysis of spatial patterns in global forest fragmentation and cover trends at a 5 km scale from 2000 to 2020 shows that 48% of forest grid cells experienced stable or increasing forest cover, while the remaining 52% saw a decline (Fig. S9A). In regions where forest cover remained stable or increased, the connectivity-focused CFI and structure-focused SFI indicate

fragmentation increased in only 5% and 10% of these areas, respectively. In contrast, the aggregation-focused AFI suggests increased fragmentation in 32% of these areas, highlighting its tendency to interpret forest cover increases as reduced aggregation (Fig. S11).

In regions experiencing forest cover loss, the CFI and AFI report increased fragmentation in 94% and 74% of grid cells, respectively. By contrast, the SFI indicates increased fragmentation in only 52% of these areas, resulting in notable discrepancies: The SFI disagrees with the CFI and AFI in 42% and 37% of forest grids with declining cover, respectively. These discrepancies (red- and orange-colored regions in Fig. S9A) are most prevalent in pan-tropical regions, such as the Amazon, Congo, and Indonesian rainforests, as well as in boreal zones. Geographically, the most substantial discrepancies between the CFI and SFI are found at low latitudes (from 15°N to 25°S) and high latitudes >50°N (Fig. S9B). The AFI disagrees with the CFI in 27% of grid cells where forest cover has decreased, following a similar latitudinal pattern but with a smaller magnitude of change (Fig. S9). This analysis underscores the limitations of structure-focused metrics such as the SFI, which can underestimate fragmentation trends in deforested areas by equating reductions in the number and size of patches with decreased fragmentation. This assumption fails to capture the ecological reality of habitat fragmentation, where patch loss often leads to greater isolation and reduced connectivity, exacerbating the negative impacts on biodiversity and ecosystem functionality (*11*).

Quantifying contributions of different drivers to increased fragmentation

To investigate the drivers of forest fragmentation, we distinguished between permanent land conversions, like deforestation and urban expansion, and temporary disturbances, such as forestry operations and wildfires. Curtis et al. 2018 developed a global map of forest loss drivers, derived from 30m-resolution Google Earth imagery between 2000 and 2015 using a machine-learning algorithm (*8*). This dataset was later updated on Global Forest Watch using the same methodology to extend coverage to 2000-2023 (Fig. 23; https://data.globalforestwatch.org/documents/gfw::tree-cover-loss-by-dominant-driver-2023/about). Details regarding validation and uncertainty assessments of the driver estimations are provided in Curtis et al. (2018).

Using these datasets, we quantified the impact of different drivers on CFI-based fragmentation trends for the periods 2000-2015 (Fig. S12) and 2000-2023 (Fig. 3). We extracted the primary driver of forest loss and fragmentation for each grid cell and classified them into seven categories based on the dominant cause and fragmentation trends:

- **Uncertain:** cases where the cause of increased fragmentation could not be determined.
- **Wildfire:** areas where fragmentation is driven by natural fire-related disturbances without human-induced land conversion.
- **Forestry:** Large-scale forestry activities that cause fragmentation but show signs of regrowth.
- **Shifting agriculture:** transient agricultural conversion with eventual regrowth.
- **Deforestation:** permanent conversions to non-forest land uses, such as agriculture, mining or infrastructure projects.
- **Urbanization:** expansion of urban areas.
- **No increase:** regions where fragmentation did not increase over the past 20 years.

Comparison of forest loss and fragmentation between protected and non-protected areas.

Forests within protected areas are expected to experience fewer human disturbances due to conservation policies and lower population densities, which should result in reduced deforestation and degradation compared to non-protected forests. To assess whether these reduced disturbances in protected areas result in decreased forest fragmentation, we used the World Database on Protected Areas (WDPA) (*40*). We identified forest grid cells within protected areas established before 2010, allowing at least a decade for the effects of protection to manifest (Fig. S20). We then categorized forests into three groups:

- **Strictly protected areas:** including the most stringent IUCN protection categories (Ia: strict nature reserve, Ib: wilderness area, and II: national park).
- **Protected areas:** includes IUCN categories that allow for some resource use (III: natural monument or feature, IV: habitat or species management area, V: protected landscape or seascape, and VI: protected area with sustainable use of natural resources).
- **Non-protected areas:** forests outside any official protection status.

To ensure fair comparisons between fragmentation rates inside and outside protected areas, we implemented a matching procedure that created counterfactuals outside protected areas based on environmental and social-economic covariates (*42, 44-46*). For this analysis, we combined the strictly protected and protected categories into a single "protected" group. We measured changes in forest fragmentation using the change in the Connectivity-based Fragmentation Index ($\Delta CFI = CFI_{2020} - CFI_{2000}$). To address spatial autocorrelation, we only included forest grid cells at least 40 km apart (*45, 46, 63*), as Moran's I analysis indicated negligible spatial autocorrelation in model residuals at this distance (Fig. S14). The spatial model used here predicts protection status (whether a grid cell is inside a protected area or not) using a binomial logistic regression model with

environmental and socio-economic covariates, including mean annual temperature (*64*), annual precipitation (*64*), temperature seasonality (*64*), precipitation seasonality (*64*), aridity (*64*), population density (*65*) and fire frequency (*66*) from 2000 to 2020, and accessibility to cities in 2015 (*67*).

We employed a control intervention with matching analysis design (*46, 68, 69*) to compare protected vs. non-protected areas, defining control units as forest grid cells outside protected areas. To identify potential cofounding variables influencing protection status, we performed a binomial logistic regression and assessed multicollinearity among predictor variables, retaining only those with Variance Inflation Factor (VIF) < 0.65 (*70, 71*). Model selection was optimized using backward and forward stepwise regression based on the Akaike Information Criterion (AIC) (*70*). The final model included average values of mean annual temperature (*64*), annual precipitation (*64*), population density (*65*) and fire frequency (*66*) from 2000 to 2020, and accessibility to cities in 2015 (*67*).

Using the MatchIt package (*72*) in R, we applied Propensity Score Matching (*45, 46, 68-70*) to create a statistically balanced counterfactual sample for evaluating the impact of protection on forest fragmentation. Diagnostic statistics confirmed the robustness of the matching process (Fig. S15-16), ensuring that the covariate imbalance index for each variable after matching was within acceptable limits (< 25%) (*46, 73, 74*). This matching procedure resulted in a new grid cell category: "matched non-protected". We then compared CFI change and the primary drivers of fragmentation across the following four categories: *Strictly protected*, *Protected*, *Matched non-protected* (statistically similar non-protected areas) and *All non-protected areas*. Since the fragmentation rates across different categories did not follow a Gaussian distribution, we used the Kruskal-Wallis test followed by post-hoc Mann-Whitney U tests (*75*) to assess differences between groups.

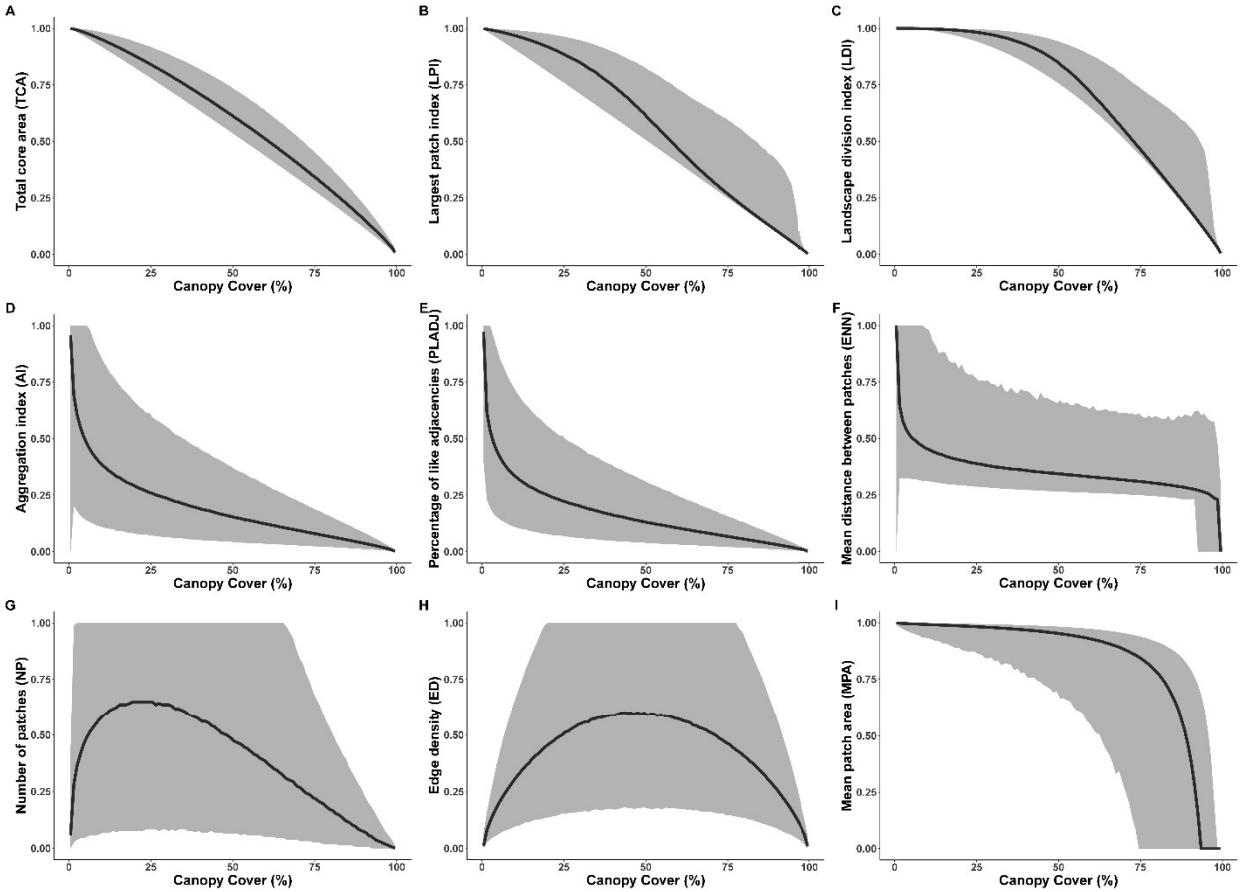

Fig. S1 | Relationship between forest cover and normalized fragmentation metrics. This figure illustrates the relationship between forest canopy cover and nine normalized fragmentation metrics based on global forest data from the year 2000. Each normalized fragmentation metric scaled from 0 to 1, with larger values indicate higher fragmentation, see Tables 1 and S1 for details. **A**, Total core area (TCA). **B**, Largest patch index (LPI). **C**, Landscape division index

(LDI). **D**, Aggregation index (AI). **E**, Percentage of like adjacencies (PLADJ). **F**, Mean Euclidean distance between patches (ENN). **G**, Number of patches (NP). **H**, Edge density (ED). **I**, Mean patch area (MPA). In each panel, the solid black line represents the median trend, while the shaded area denotes the 2.5th to 97.5th percentiles, capturing the variability in fragmentation metrics across different levels of forest cover.

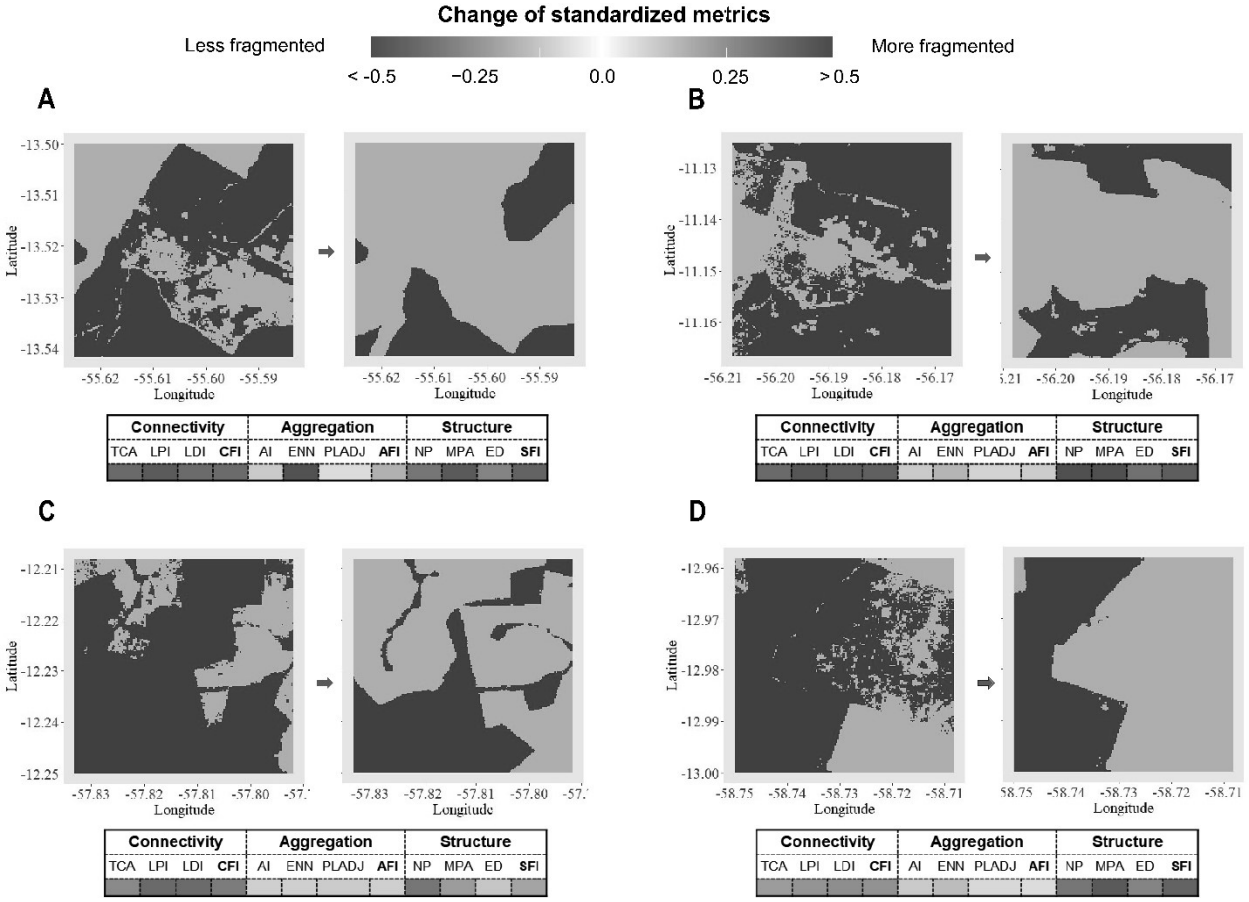

Fig. S2 | Observed deforestation and fragmentation trends in the Amazon (2000-2020). This figure shows observed deforestation across four sites in the Amazon from 2000 (left panels) to 2020 (right panels). Each site illustrates different patterns of forest loss and fragmentation. In all cases, connectivity-focused fragmentation metrics indicate an increase in fragmentation (red), while structure-focused metrics suggest a decline (blue), as they primarily measure patch count rather than spatial configuration. Aggregation-focused metrics exhibit mixed trends, reflecting variations in spatial clustering and edge distribution. The color intensity in the metric tables represents the magnitude of change, with darker shades indicating stronger fragmentation shifts.

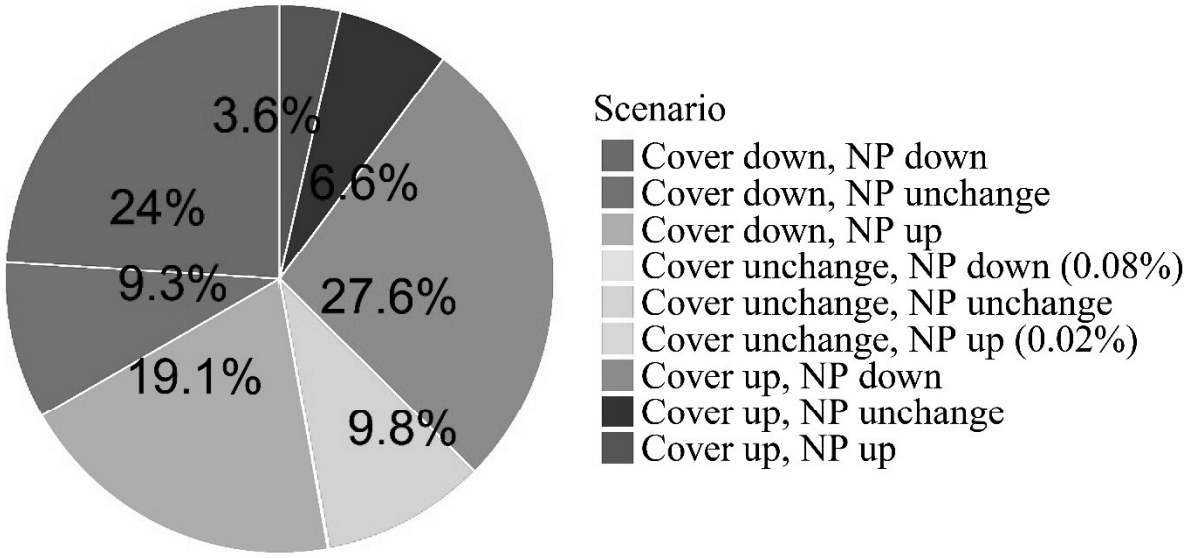

780 **Fig. S3 | Proportion of landscape change scenarios in global forests between 2000 and 2020, based on changes in forest cover and the number of patches (NP).** Both forest cover and NP can either remain unchanged, decline, or increase, leading to a total of nine possible scenarios. Each colored segment in the pie chart represents the percentage of forest grid cells falling into each scenario.

785

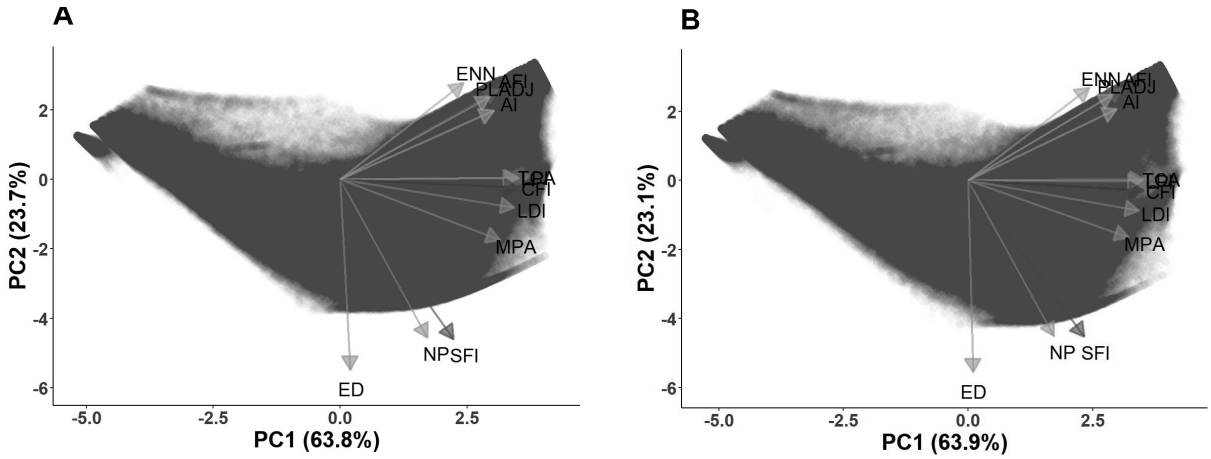

Fig. S4 | PCA space of fragmentation metrics. A, PCA biplot of 12 fragmentation metrics across all grid cells with forest cover > 0 in the year 2000. **B**, The same PCA analysis for the year 2020. Connectivity-focused metrics are shown in red, aggregation-focused metrics are in orange, and structure-focused metrics are in blue. The integrated indices—Connectivity-based Fragmentation Index (CFI), Aggregation-based Fragmentation Index (AFI), and Structure-Focused Index (SFI)—are emphasized in darker shades within their respective groups. A Pair-wise Multivariate Analysis of Variance (MANOVA) confirms significant differences among loadings of these three metric groups ($p < 0.001$), indicating that connectivity, aggregation, and structure metrics form distinct clusters in both years.

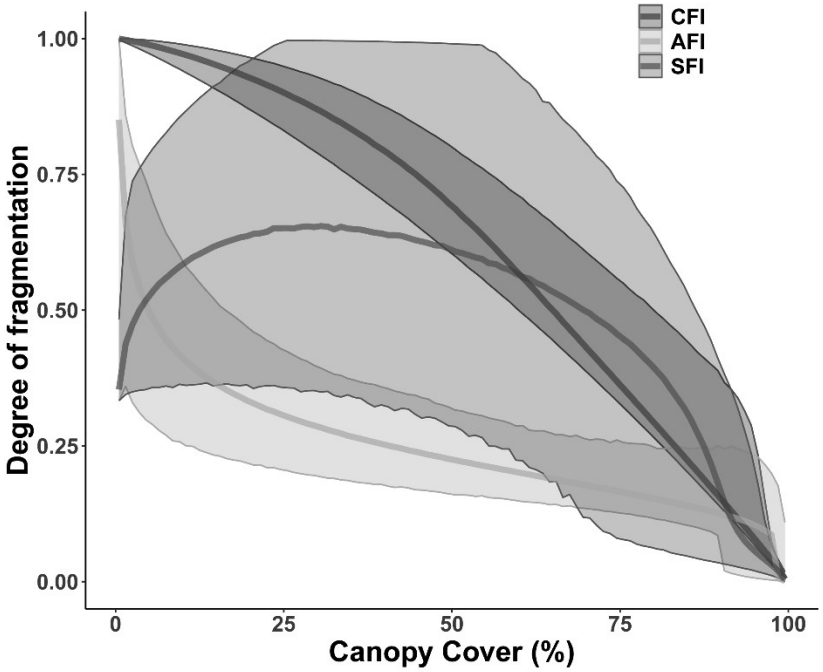

Fig. S5 | Relationship between fragmentation and canopy cover. This figure illustrates the relationship between the degree of forest fragmentation and canopy cover (%) for all grid cells with forest cover > 0 in 2020, based on the CFI, AFI and SFI. The solid line represents the median degree of fragmentation at each canopy cover percentage, while the shaded areas indicate the 2.5th and 97.5th percentiles, capturing the variability in fragmentation levels.

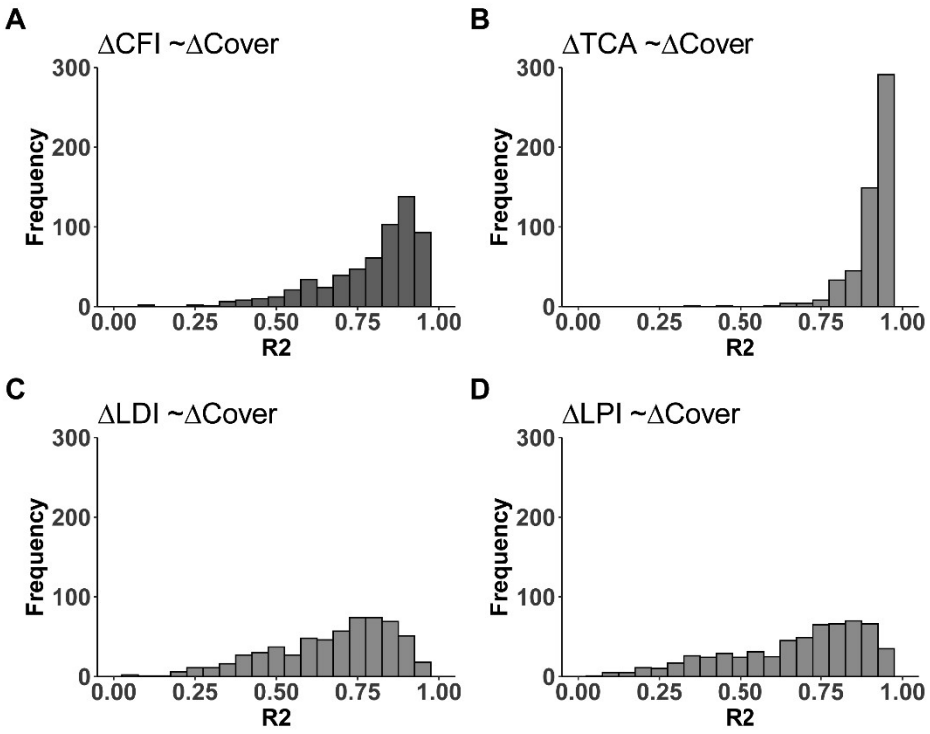

Fig. S6 | Relationship between changes in connectivity-focused fragmentation metrics and forest cover change. This figure presents histograms of the coefficients of determination (R^2 values) from simple linear regression models predicting changes in connectivity-focused fragmentation metrics as a function of forest cover change across 610 ecoregions (each has at least 50 forest grid cells inside) from 2000 to 2020. **A-D,** Relationships between forest cover change and changes in Connectivity-based Fragmentation Index (CFI) (**A**), Total Core Area (TCA) (**B**), Landscape Division Index (LDI) (**C**), and Largest Patch Index (LPI) (**D**).

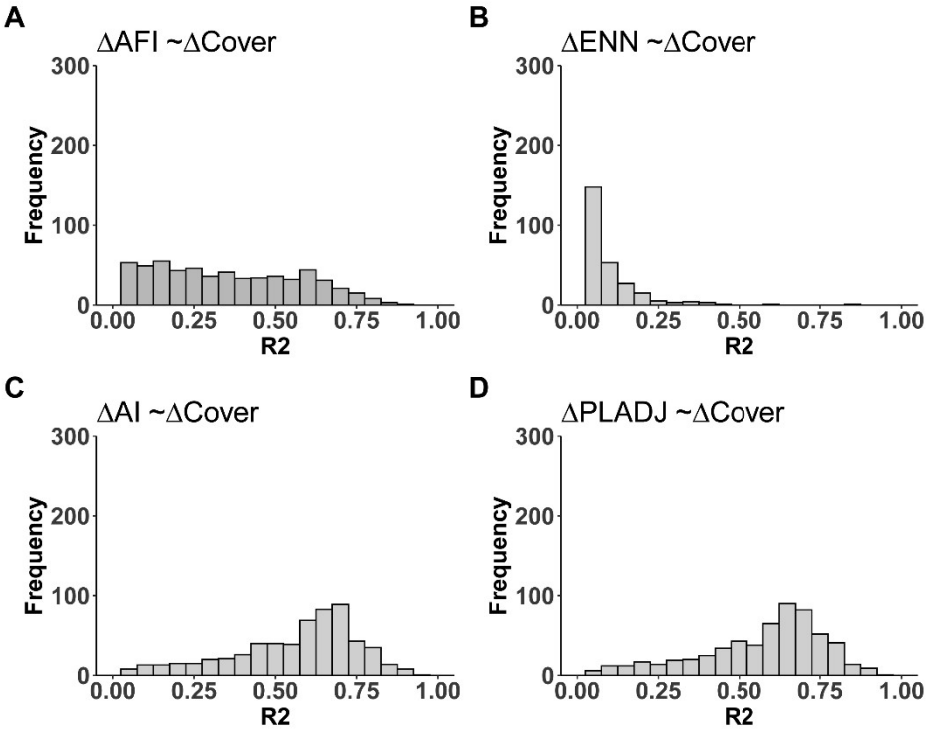

Fig. S7 | Relationship between changes in aggregation-focused fragmentation metrics and forest cover change. This figure presents histograms of the coefficients of determination (R^2 values) from simple linear regression models predicting changes in aggregation-focused fragmentation metrics as a function of forest cover change across 610 ecoregions (each has at least 50 forest grid cells inside) from 2000 to 2020. **A-D,** Relationships between forest cover change and changes in Aggregation-based Fragmentation Index (AFI) (**A**), Mean of Euclidean nearest-neighbor distance (ENN) (**B**), Aggregation Index (AI) (**C**), and Percentage of Like Adjacencies (PLADJ) (**D**).

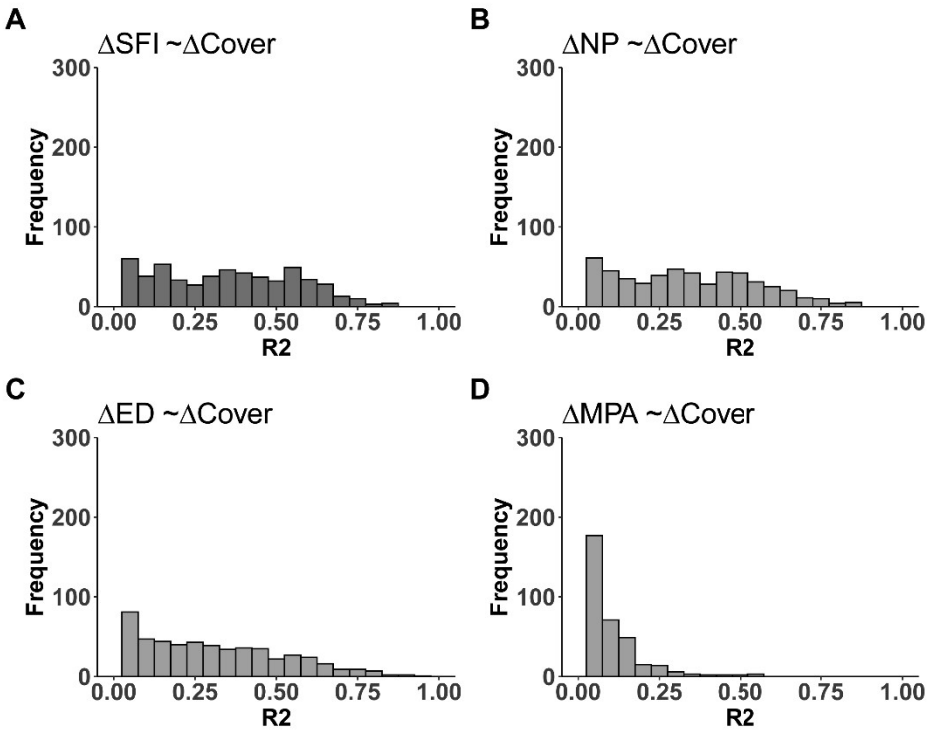

Fig. S8 | Relationship between changes in structure-focused fragmentation metrics and forest cover change. This figure presents histograms of the coefficients of determination (R^2 values) from simple linear regression models predicting changes in structure-focused fragmentation metrics as a function of forest cover change across 610 ecoregions (each has at least 50 forest grid cells inside) from 2000 to 2020. **A-D,** Relationships between forest cover change and changes in Structure-based Fragmentation Index (SFI) (**A**), Number of Patches (NP) (**B**), Edge Density (ED) (**C**), and Mean Patch Area (MPA) (**D**).

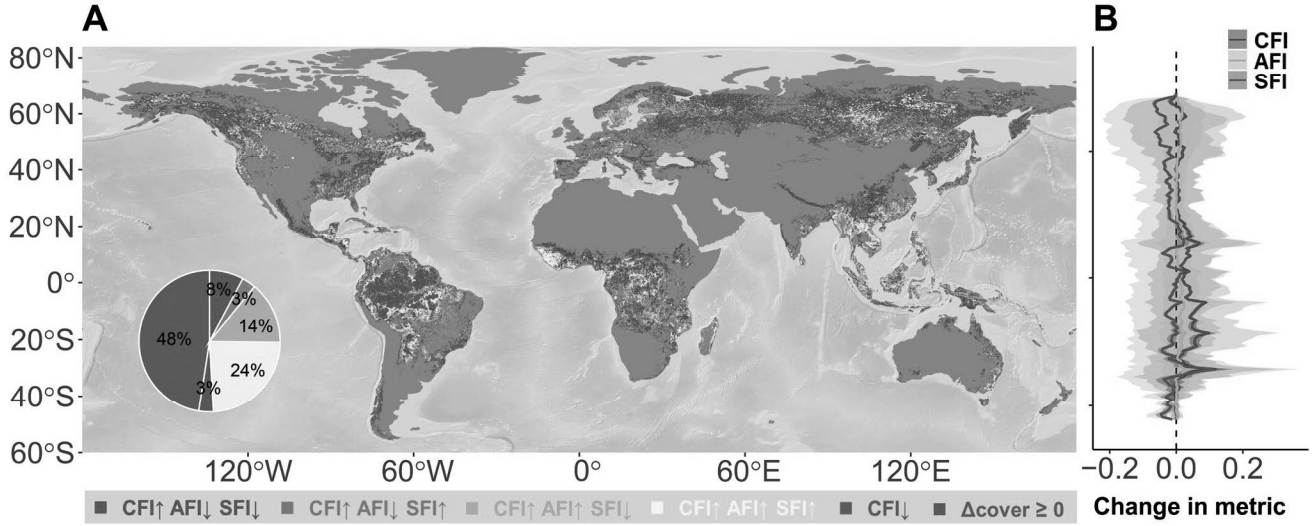

Fig. S9 | Global patterns of forest fragmentation change from 2000 to 2020. A, Map of six landscape-change categories at 2.5 arc-min (~5 km) resolution (in geographic coordinates EPSG: 4326). Blue pixels: no forest loss. In all other regions (purple, yellow, orange, brown, red), forest cover has declined. Purple: declines in CFI. Yellow: All three metrics (CFI, AFI and SFI) agree on increased fragmentation. Orange: CFI and AFI indicate increased fragmentation, but SFI reports a decrease (as in Fig. 1F). Brown: CFI and SFI indicate increased fragmentation, while AFI shows a decrease.

Red: CFI suggests increased fragmentation, whereas both AFI and SFI indicate decreased fragmentation, representing mismatch scenarios similar to Fig. 1C. **B**, Latitudinal distribution of changes in CFI, AFI and SFI, showing the means (solid line), confidence intervals (± 3 standard errors, dark shadow) and standard deviations (light shadow).

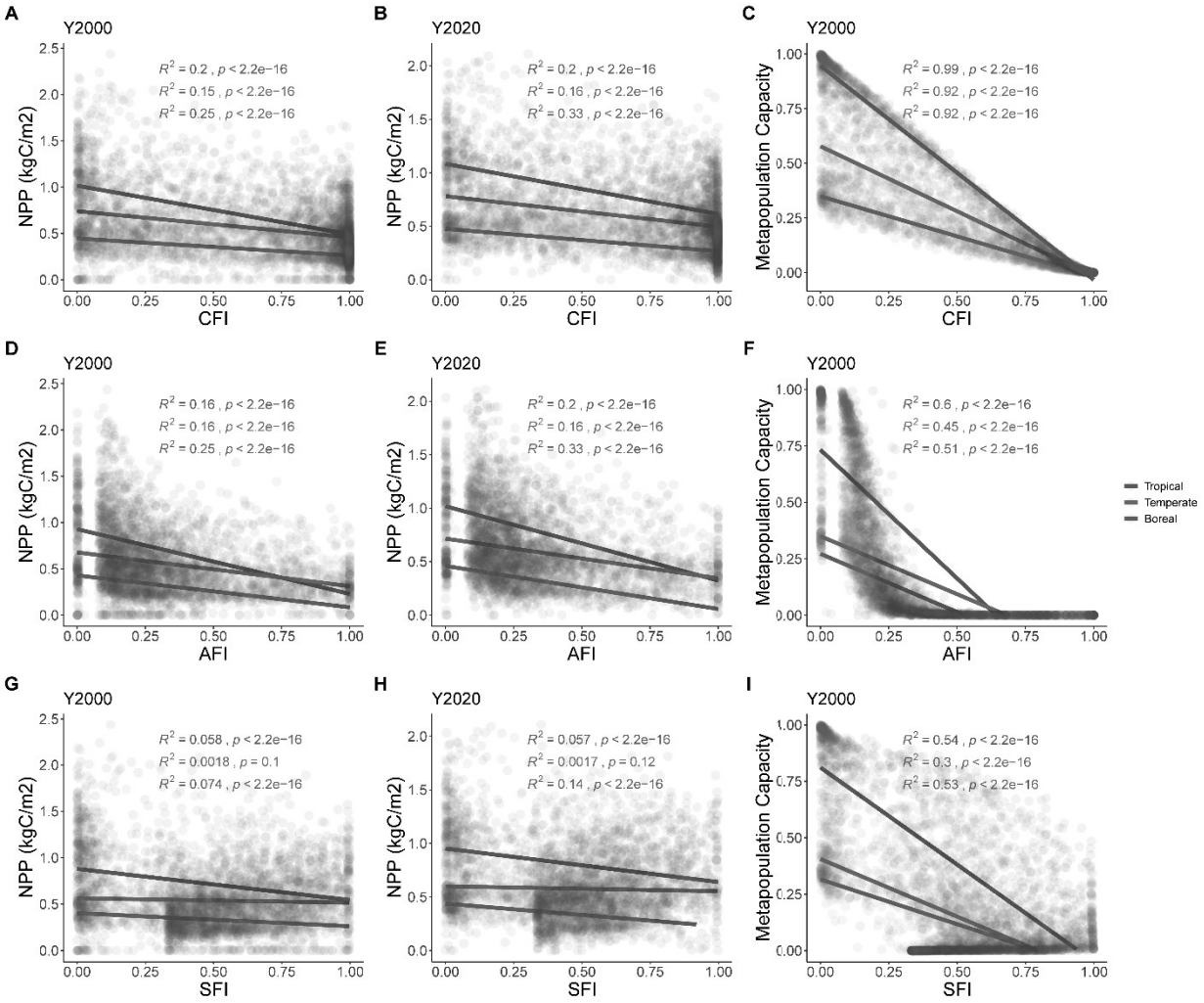

Fig. S10 | Relationships between fragmentation metrics (CFI, AFI or SFI) and net primary productivity (NPP) or Metapopulation Capacity (MPC) across different biomes. A-C, Relationships between NPP (year 2000), NPP (2020), and MPC (2000) with CFI for the respective year. **D-F,** Relationships between NPP (year 2000), NPP (2020), and MPC (2000) with AFI. **G-I,** Relationships between NPP (year 2000), NPP (2020), and MPC (2000) with SFI. Insets show coefficients of determination (R^2) and p-values from linear regression. NPP data were derived from the MODIS MOD17A3HGF.061 product at 500m resolution, aggregated to 5 km resolution for analysis (*76*).

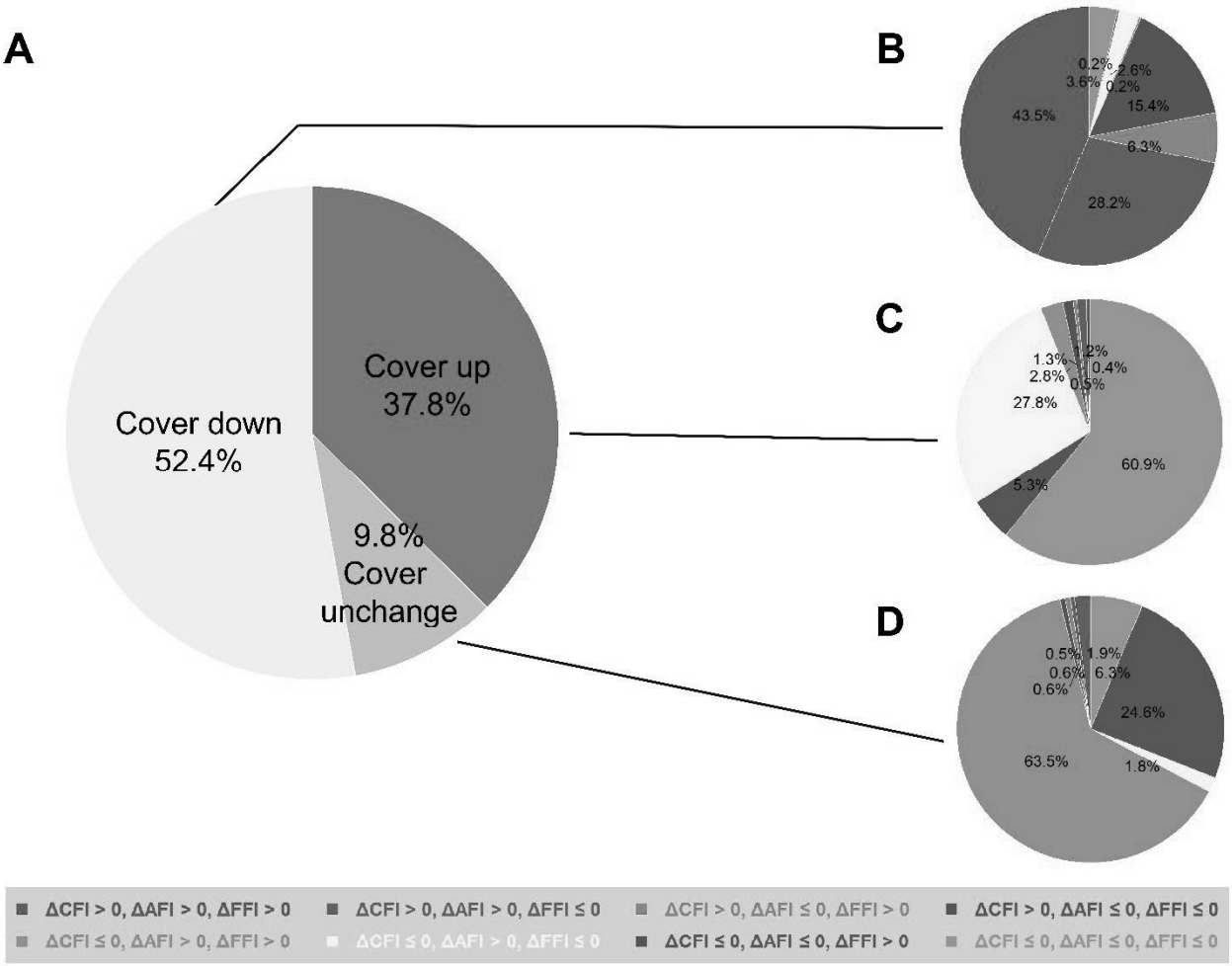

Fig. S11 | Changes in fragmentation metrics (CFI, AFI and SFI) in relation to forest cover change between 2000 and 2020. A, Global distribution of forest cover change. This pie chart represents the proportion of forest grid cells where canopy cover has decreased (52.8%), increased (37.4%), or remained unchanged (9.8%). **B-D,** Agreement and discrepancies among fragmentation metrics. Proportion of grid cells for which the CFI, AFI and SFI agree or disagree on fragmentation trends across regions where forest cover has decreased (**B**), increased (**C**), and remained unchanged (**D**). Each color represents a specific combination of metric trends, highlighting areas where CFI, AFI, and SFI indicate similar or conflicting patterns in fragmentation changes. The legend at the bottom categorizes these trends based on whether fragmentation increased (>0) or remained stable/decreased (≤0) according to each metric.

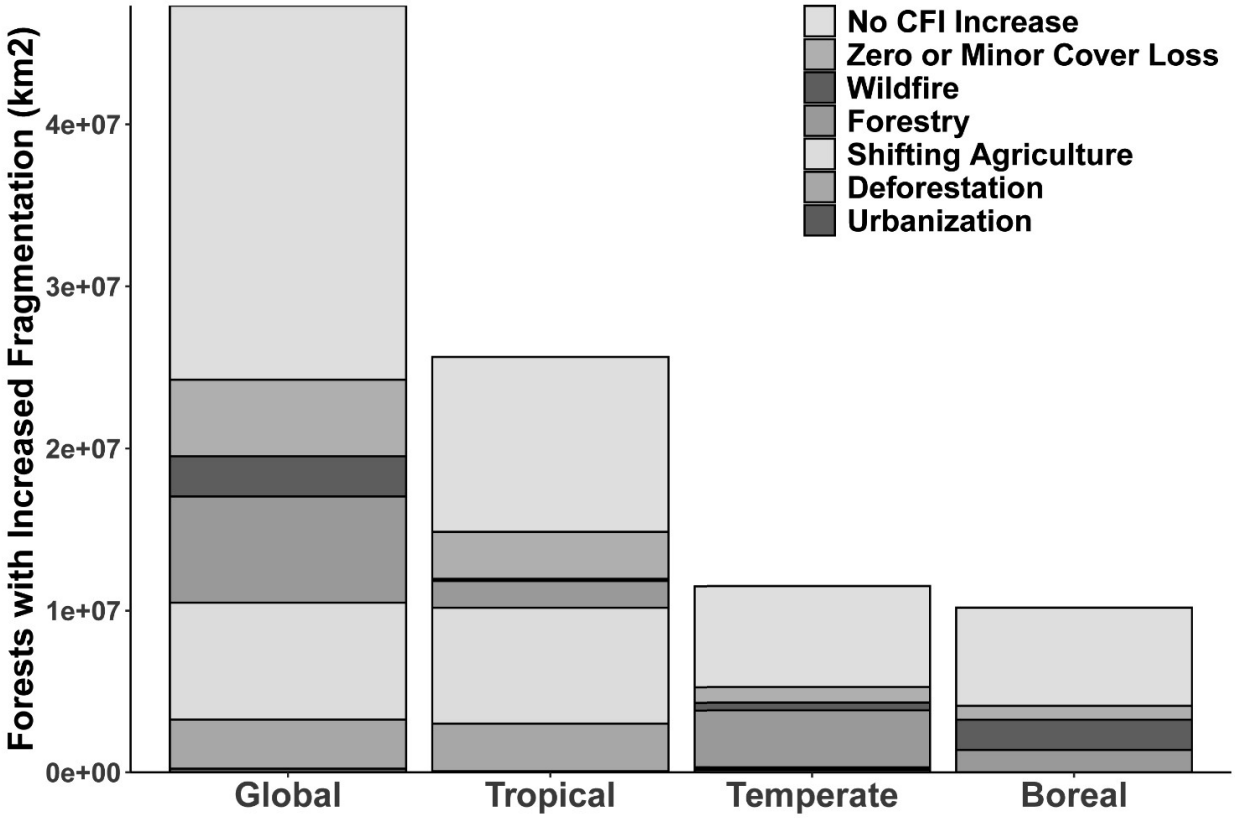

Fig. S12. Drivers of forest fragmentation trends (2000–2020) across biomes (same as Fig. 4 but using the 2000-2015 instead of the 2000-2023 driver map). Total area of forest regions (grid cells with >30% canopy cover) affected by different fragmentation drivers at global and biome scales. “No CFI increase” represents forest regions where fragmentation levels have remained stable or decreased. "Zero or minor cover loss" includes areas where fragmentation slightly increased due to unknow cause but with minor or no forest cover loss. All other categories represent regions with increased fragmentation driven by specific factors, including i) “Wildfire”, where forest burning occurred without subsequent human conversion or agricultural activity, ii) “Forestry”, representing large-scale harvesting within managed forests with signs of regrowth, iii) “Shifting agriculture”, referring to small- to medium-scale forest conversion for agriculture, later abandoned and followed by forest regrowth, iv) “Deforestation”, characterized by permanent forest loss due to commodity-driven activities such as agriculture, mining, or energy infrastructure, and v) “Urbanization”, where forests have been converted for urban expansion. The drivers are arranged from “Wildfire” (top) to “Urbanization” (bottom) to reflect the increasing degree of irreversible forest loss.

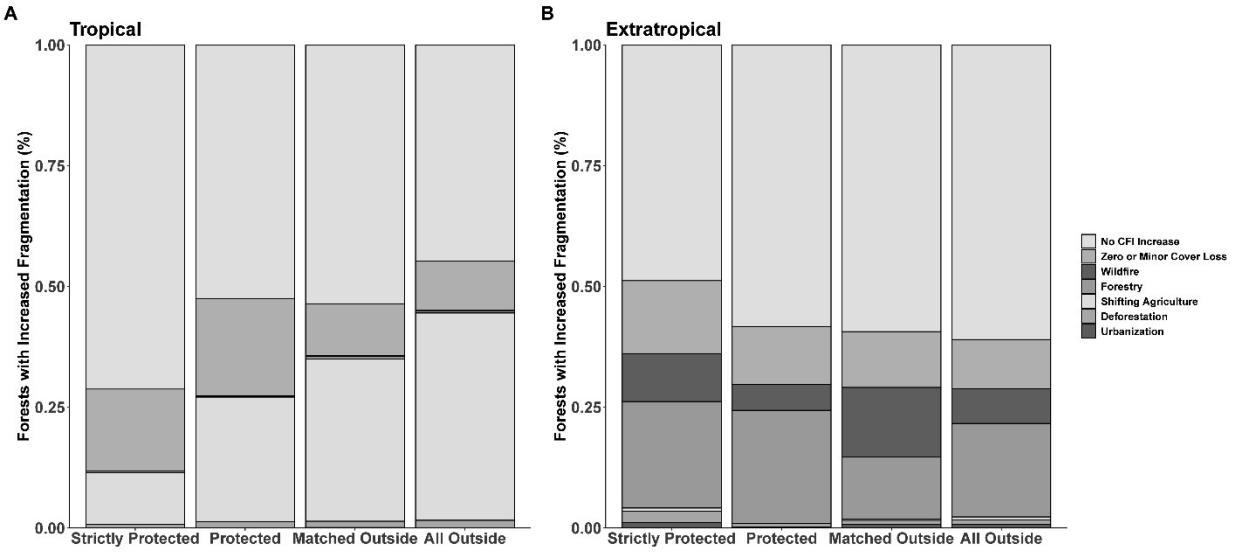

Fig. S13. Forest fragmentation trends (2000–2020) inside and outside protected areas (same as Fig. 4B,D but using the 2000-2015 instead of the 2000-2023 driver map). Proportions of forest regions experiencing fragmentation due to different drivers across different protection categories in tropical (**A**) and extratropical (**B**) regions. "No CFI increase" represents areas where fragmentation levels have remained stable or decreased. "Zero or minor cover loss" includes areas where fragmentation slightly increased due to unknow cause but with minor or no forest cover loss. All other categories represent regions with increased fragmentation driven by specific factors such as forestry, shifting agriculture, deforestation, or urbanization.

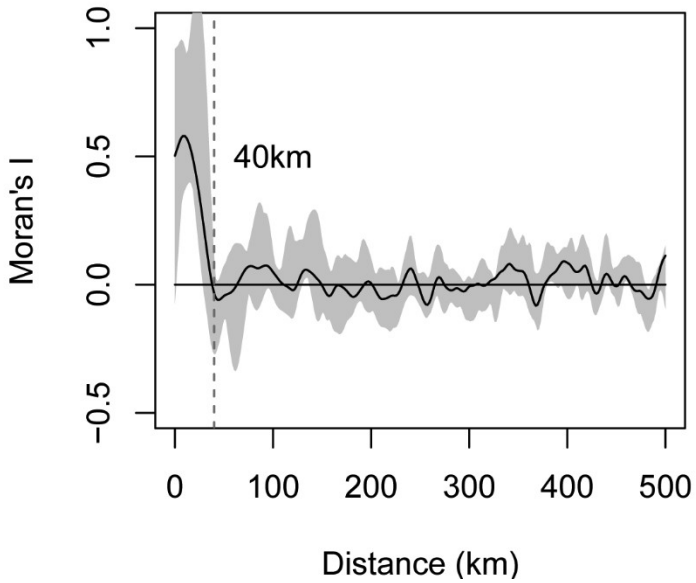

Fig. S14 | Spatial autocorrelation in protection status predictions. This figure presents the residual spatial autocorrelation (Moran's I) when predicting protection status (whether a grid cell is inside a protected area or not) using a binomial logistic regression model with environmental and socio-economic covariates, including mean annual temperature, annual precipitation, temperature seasonality, precipitation aridity, population density and fire frequency from 2000 to 2020, and accessibility to cities in 2015. The black line represents Moran's I values across different distances. The shaded region indicates the confidence interval obtained from 100 bootstrap samples. The red dashed line at ~40 km marks the threshold distance where spatial autocorrelation becomes negligible. Since positive spatial autocorrelation was observed up to ~40 km, this distance was applied as a buffer radius in the spatially buffered sampling for modeling, ensuring that data points used in the analysis are spatially independent.

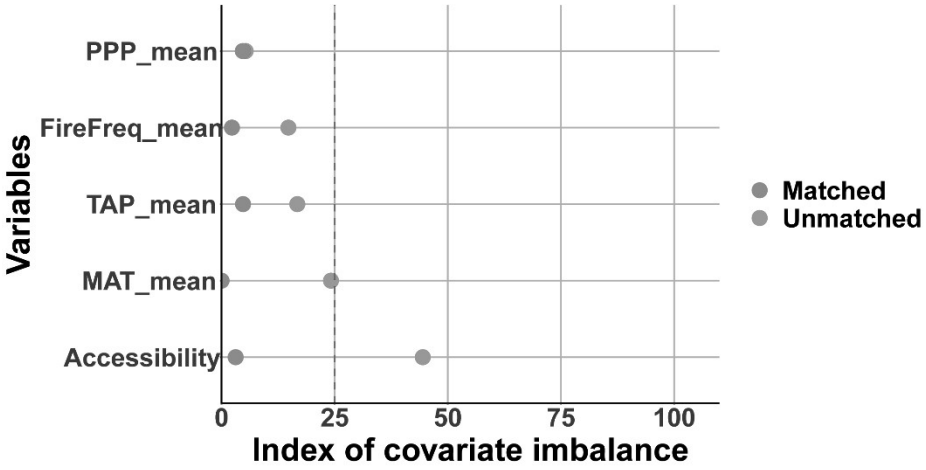

Fig. S15 | Covariate imbalance before and after the matching procedure. The covariates used in the matching model include mean annual temperature (MAT_mean), annual precipitation (TAP_mean), population density (PPP_mean) and fire frequency (fireFreq_mean) from 2000 to 2020, and accessibility to cities in 2015 (Accessibility). The index of covariate imbalance quantifies the degree of imbalance for each variable, with the red dashed line at 25% representing an acceptable threshold. The results indicate that before matching (blue), several covariates exhibit high imbalance, particularly Accessibility and MAT_mean. After matching (red), all covariates are well balanced, ensuring a more robust comparison between protected and non-protected areas.

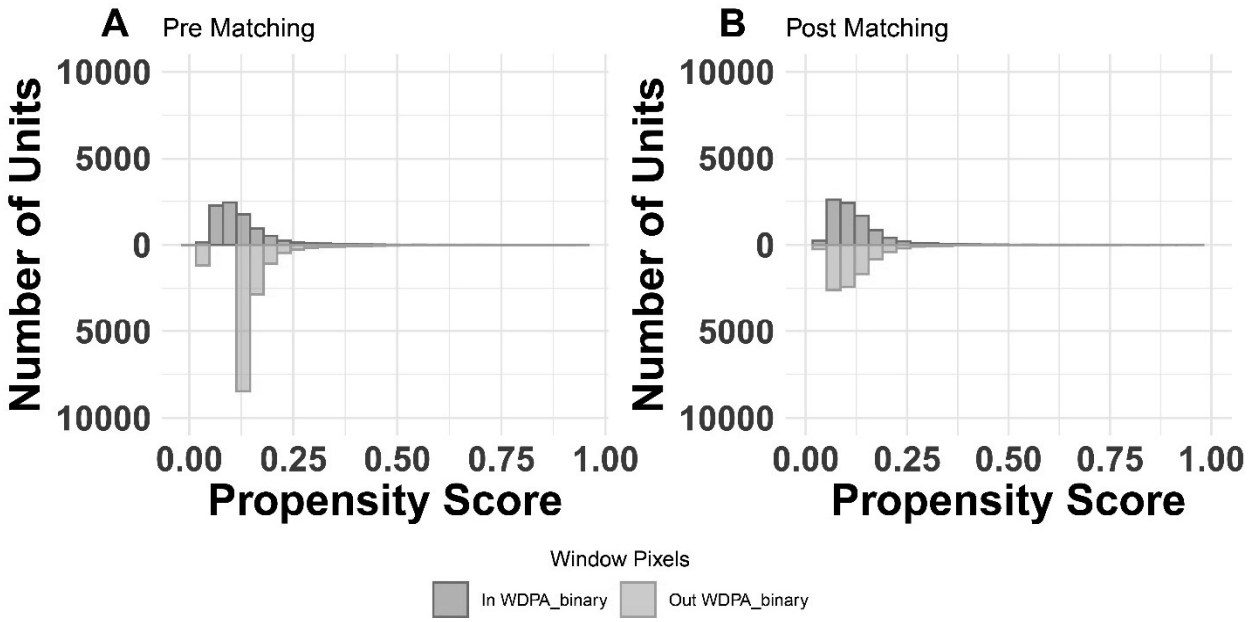

Fig. S16 | Distribution of propensity scores before and after matching. This figure illustrates the distribution of propensity scores for forest grid cells inside (green) and outside (yellow) protected areas before and after applying the matching procedure. **A**, Pre-Matching: A clear imbalance in propensity scores is observed between protected (green) and non-protected (yellow) areas, indicating systematic differences in environmental and socio-economic covariates. **B**, Post-Matching: After matching, the distributions of propensity scores in protected and non-protected areas are more aligned, ensuring a balanced comparison between the two groups. This balance improvement confirms that the matching approach successfully reduces confounding effects, allowing for a more robust evaluation of the impact of protected areas on forest fragmentation.

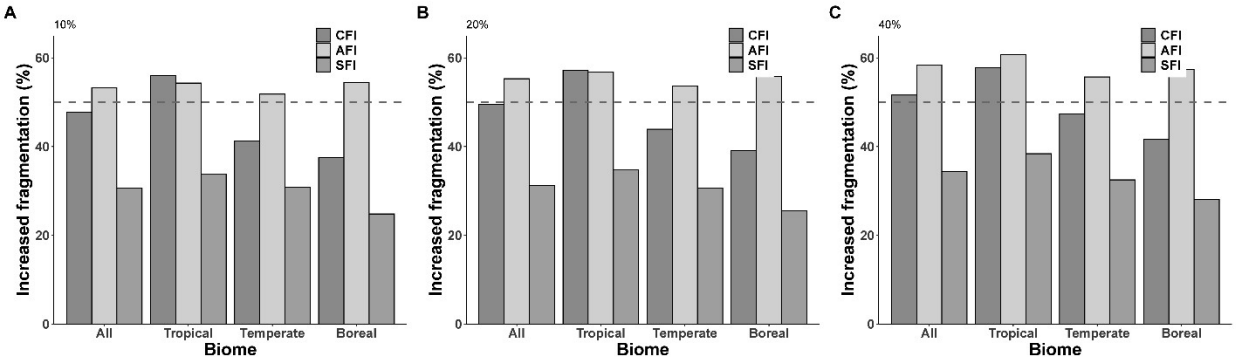

Fig. S17 | Forest areas with increased fragmentation under different forest cover thresholds. Proportion of forest grid cell areas with increased fragmentation between 2000 and 2020 at 2.5 arc-second (~5 km) resolution, based on the CFI, AFI and SFI across different biomes (All, Tropical, Temperate, and Boreal). Each panel represents different forest cover thresholds used to define forest areas: **A**, Forest cover > 10%; **B**, Forest cover > 20%; **C**, Forest cover > 40%. This figure is analogous to Figure 2D, but examines the sensitivity of fragmentation trends to different forest definitions. The results are similar across different forest cover thresholds, showing consistent fragmentation trends.

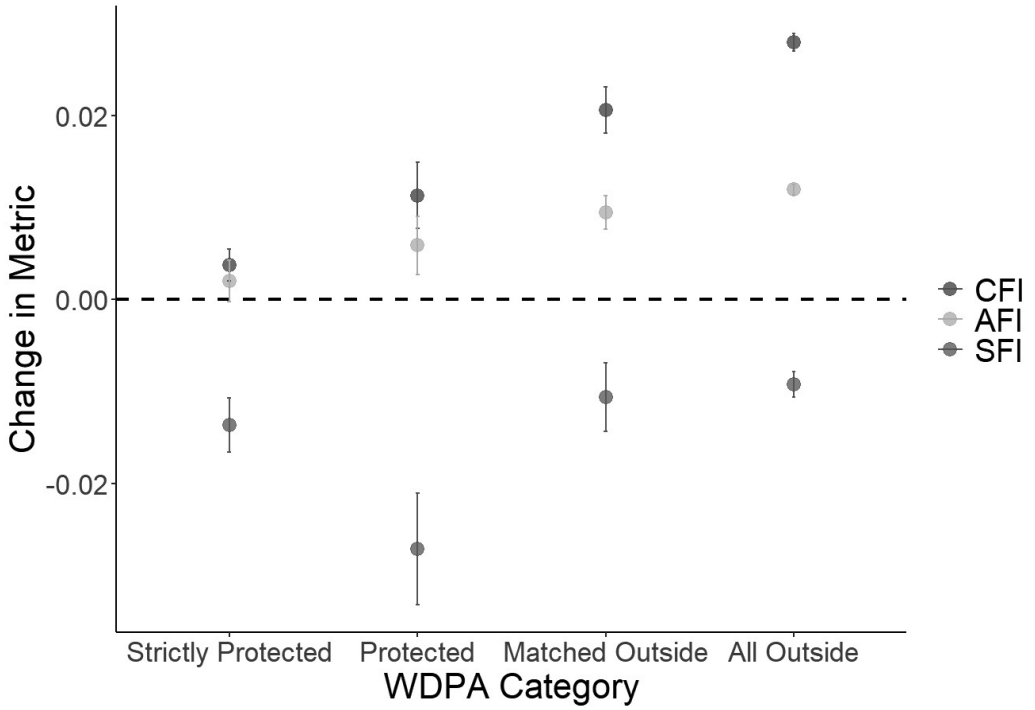

Fig. S18 | Changes in tropical forest fragmentation across protection categories. This figure compares changes in tropical forest fragmentation (mean ± 3 se) from 2000 to 2020 across different protected and non-protected areas, using the CFI, AFI and SFI. The x-axis represents protection categories based on the World Database on Protected Areas (WDPA): Strictly Protected (IUCN Categories Ia, Ib, II), Protected (IUCN Categories III–VI), Matched Outside (statistically matched non-protected areas), All Outside (all non-protected areas). The y-axis shows the change in fragmentation metric values. Values above the dashed zero line indicate increased fragmentation. Values below the line indicate decreased fragmentation. The CFI and AFI indicate increased fragmentation in non-protected areas, with the highest increase in All Outside regions. Strictly Protected areas show minimal fragmentation increases for CFI and AFI. The SFI indicates decreasing fragmentation across all protected and non-protected areas, suggesting that structure-focused metrics may underestimate actual fragmentation trends.

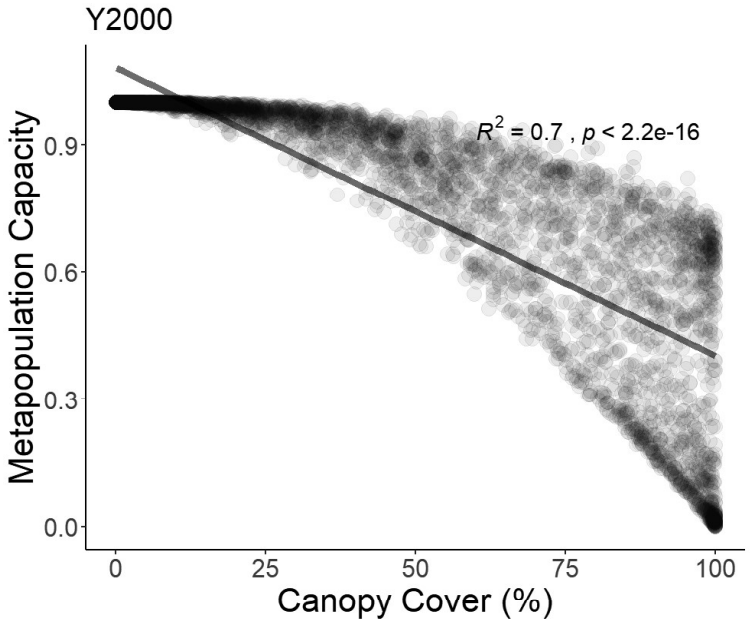

Fig. S19 | Relationship between normalized metapopulation capacity and canopy cover. Coefficients of determination (R^2) and p-value are shown for the linear regression line (red). Metapopulation capacity was normalized to range from 0 to 1. Higher values correspond to higher fragmentation and lower habitat connectivity. The relationship was derived from a 10% subsample of forest grid cells in the year 2000.

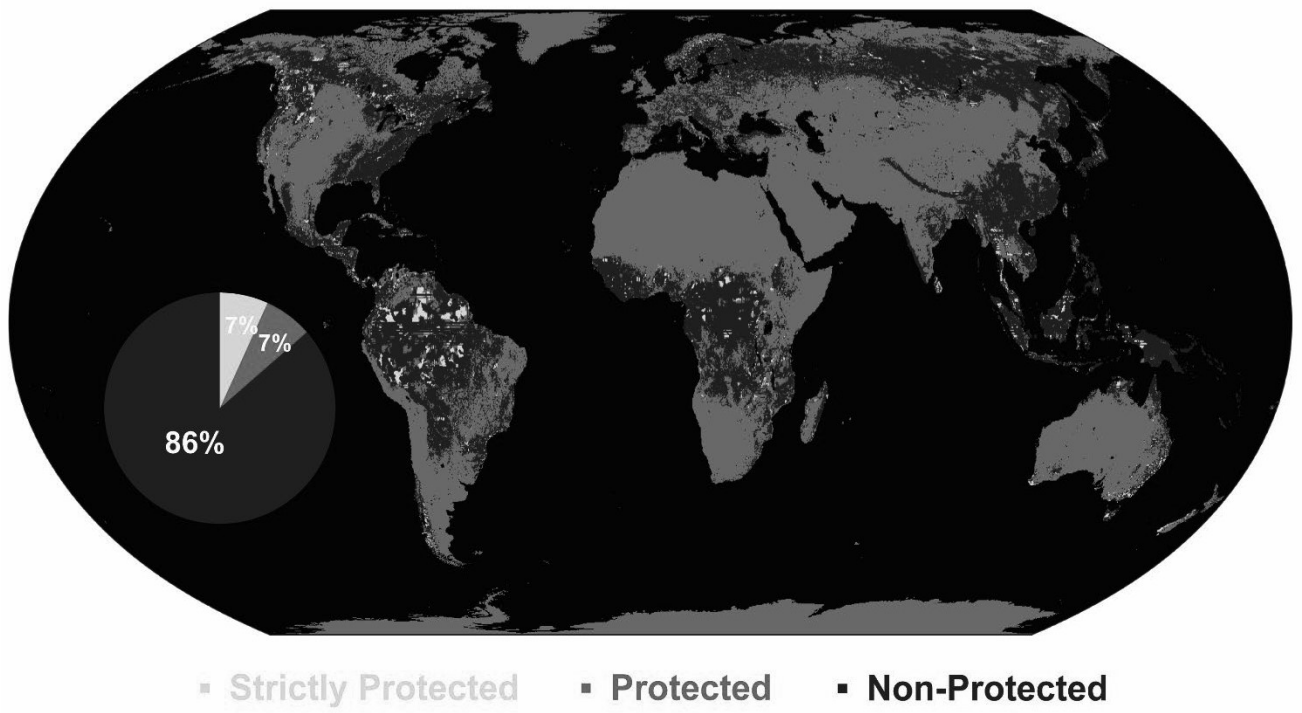

Fig. S20 | Global distribution of strictly protected, protected, and non-protected forest areas. Strictly protected forests are shown in yellow, protected forests in green, and non-protected forests in dark purple. The pie chart in the bottom left corner summarizes the proportion of forest grid cells in each category. Only protected areas established before 2010 were included in this map. Data from the World Database on Protected Areas (WDPA)

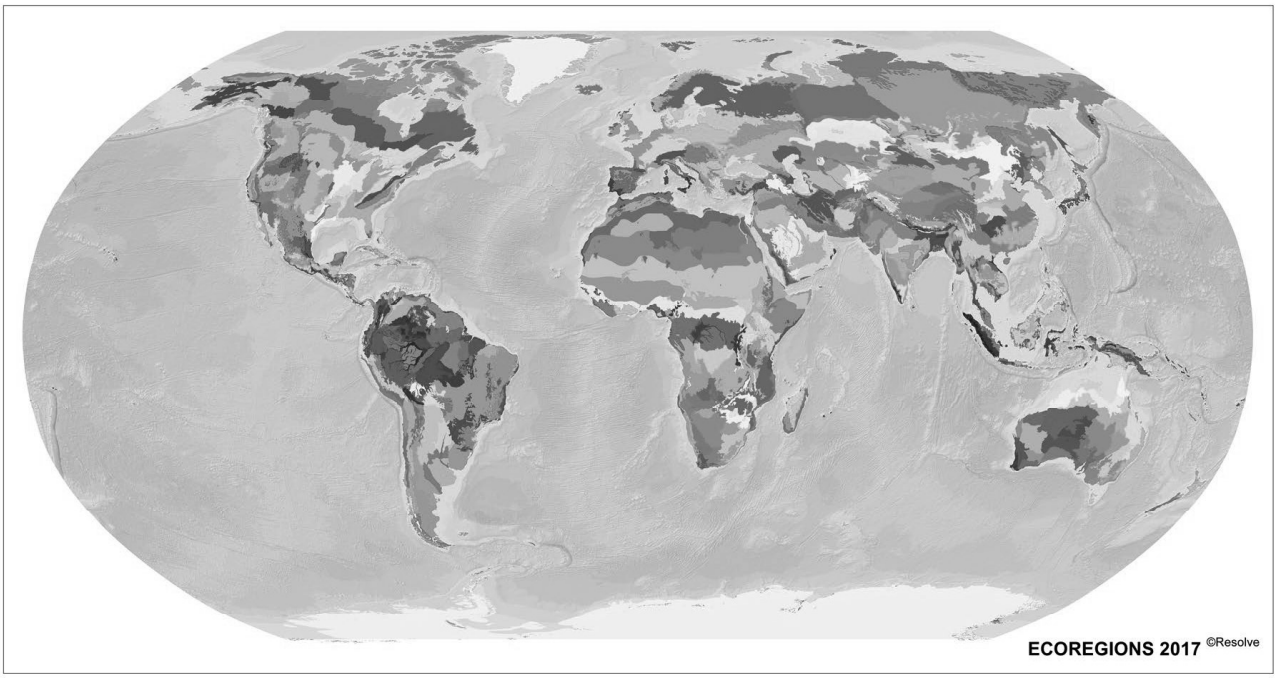

Fig. S21 | Global ecoregion map from Dinerstein et al. 2017(*41*). Different colors represent distinct ecoregions. Ecoregions are biogeographic units that reflect unique ecological and climatic characteristics, influencing biodiversity and ecosystem dynamics.

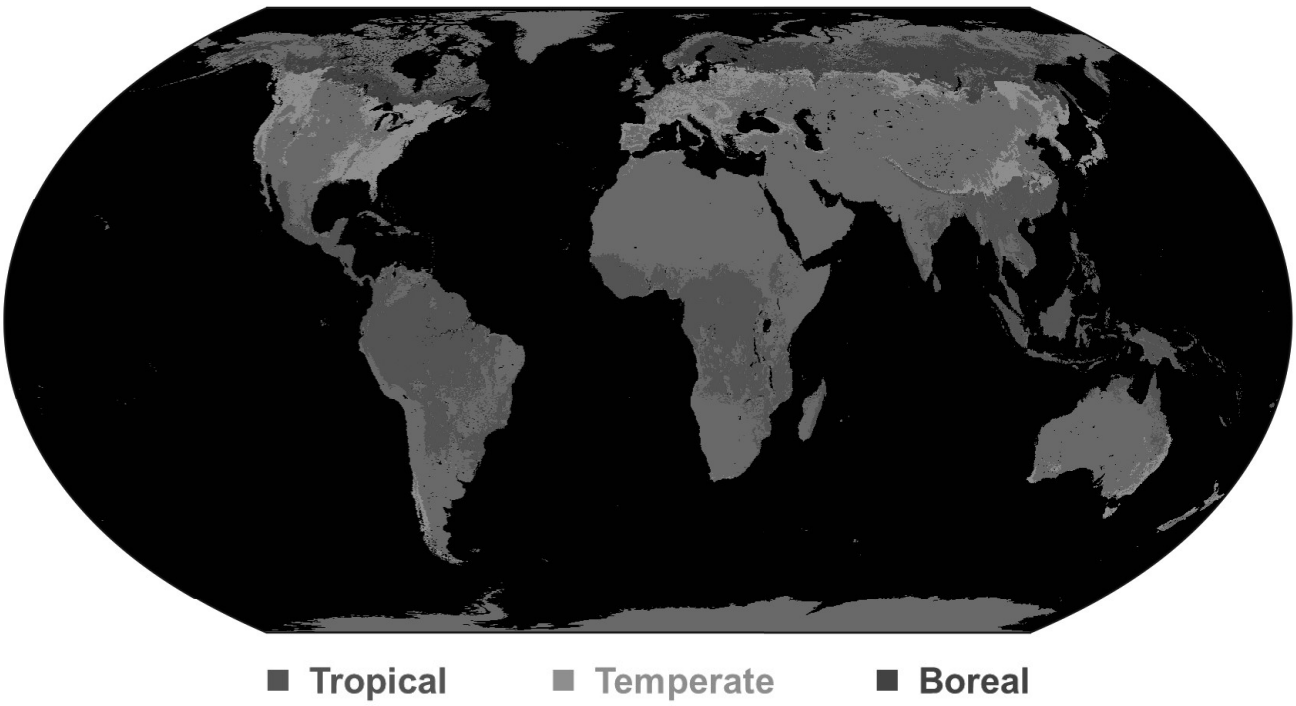

Fig. S22 | Global forest biome map. Forest biome classification was based on the terrestrial biome map from Olson et al. 2001 (*61*), which serves as the standard for WWF biome classification. The three major forest biomes are shown in different colors: tropical forests in red, temperate forests in light green and boreal forests in dark blue.

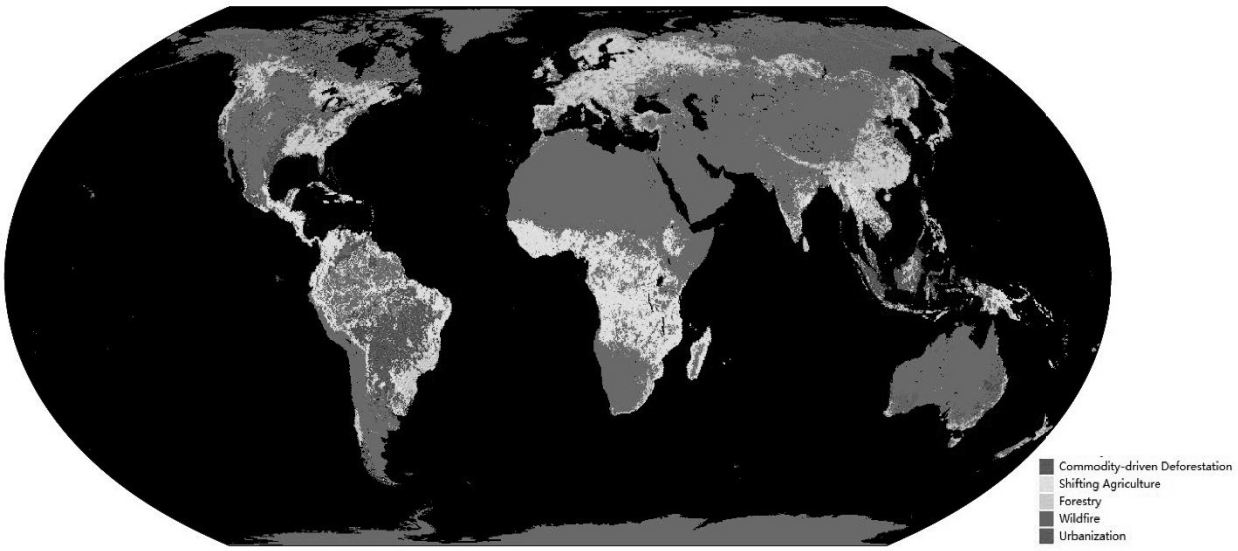

Fig. S23. Primary drivers of forest cover loss from 2000 to 2023. This map illustrates the dominant drivers of forest cover loss from 2000 to 2023, derived from Global Forest Watch based on Curtis et al. (*8*). Different colors represent specific drivers: commodity-driven deforestation (red) indicates long-term, permanent conversion of forests to agriculture, mining, or infrastructure; shifting agriculture (yellow) represents temporary forest clearing followed by regrowth; forestry (green) reflects areas affected by large-scale timber harvesting with evidence of regeneration; wildfires (orange) show areas impacted by fire without subsequent human-driven conversion; and urbanization (purple) denotes forest loss due to the expansion of urban areas.

Table S1. Overview of selected landscape-level fragmentation metrics.

Metrics	Full name	Description	Formula	Reference
TCA	Total core area	The sum of core areas of all patches belonging to forests. A cell is defined as core area if all of its neighboring cells are forests.	$TCA = \sum_{j=1}^{n} a_{ij}^{core} \times (\frac{1}{10000})$, where here a_{ij}^{core} is the core area in square meters.	McGarigal et al. (2002) (*27*)
LPI	Largest patch index	The percentage of the landscape covered by the corresponding largest patch of forest.	$LPI = \frac{\max_{j=1,\ldots,n}(a_{ij})}{A} \times 100$, where a_{ij} is the area of the patch of class i in square meters and A is the total landscape area in square meters.	McGarigal et al. (2002) (*27*)
LDI	Landscape division index	The probability that two randomly selected cells are not located in the same patch of forest.	$LDI = (1 - \sum_{j=1}^{n}(\frac{a_{ij}}{A})^2)$, where a_{ij} is the area of the patch of class i in square meters and A is the total landscape area in square meters.	Jaeger (2000) (*29*)
CFI	Connectivity-focus fragmentation index	Synthetic metric integrating TCA, LPI and LDI.	$CFI = \frac{LDI_{nor}+TCA_{nor}+LPI_{nor}}{3}$, where here LDI_{nor}, TCA_{nor}, LPI_{nor} are normalized metrics ranging from 0 to 1, and increase with fragmentation.	This paper
AI	Aggregation index	The number of like adjacencies divided by the theoretical maximum possible number of like adjacencies for forest cells.	$AI = \frac{g_{ii}}{\max[g_{ii}]} \times 100$, where g_{ii} is the number of like adjacencies based on the single-count method and max $[g_{ii}]$ is the classwise maximum possible number of like adjacencies of class i.	He et al. (2000) (*30*)
PLADJ	Percentage of Like Adjacencies	The number of adjacencies between forest cells divided by the number of adjacencies between forest and non-forests cells.	$PLADJ = (\frac{g_{ij}}{\sum_{k=1}^{m} g_{ik}}) \times 100$, where g_{ii} is the number of adjacencies between cells of class i and g_{ik} is the number of adjacencies between cells of class i and k.	McGarigal et al. (2002) (*27*)
ENN	Mean of Euclidean nearest-neighbor distance	The mean Euclidean distance to the nearest neighboring patch for each forest patch.	$ENN = mean(ENND[patch_{ij}])$, where $ENND[patch_{ij}]$ is the euclidean nearest-neighbor distance of each patch.	McGarigal et al. (2002) (*27*)
AFI	Aggregation-focus fragmentation index	Synthetic metric integrating AI, PLADJI and ENN.	$AFI = \frac{ENN_{nor}+PLADJ_{nor}+AI_{nor}}{3}$, where here ENN_{nor}, $PLADJ_{nor}$, AI_{nor} are normalized metrics ranging from 0 to 1, and increase with fragmentation.	This paper

NP	Number of patches	Number of distinct forest patches.	$NP = n_i$, where n_i is the number of patches.	McGarigal et al. (2002) (*27*)
MPA	Mean patch area	The mean of all patch areas belonging to forests.	$MPA = mean(AREA[patch_{ij}])$, where $AREA[patch_{ij}]$ is the area of each patch in hectares.	McGarigal et al. (2002) (*27*)
ED	Edge density	The length sum of all edges of forest divided by the landscape area (In our study the landscape area is the grid cell area).	$ED = \frac{\sum_{k=1}^{m} e_{ik}}{A} \times 10000$, where e_{ik} is the total edge length in meters and A is the total landscape area in square meters.	McGarigal et al. (2002) (*27*)
SFI	Structure-focused fragmentation index	Synthetic metric integrating NP, MPA and ED. This metric was called FFI in Ma et al. (2023).	$FFI = \frac{ED_{nor}+NP_{nor}+MPA_{nor}}{3}$, where here ED_{nor}, NP_{nor}, MPA_{nor} are normalized metrics ranging from 0 to 1, and increase with fragmentation.	Ma et al. (2023) (*7*)
MPC	Metapopulation capacity	A relative measure of the ability of a spatially explicit landscape to support long-term species persistence based on connectivity of habitat.	$MPC = \lambda_m$ $m_{ij} = \begin{cases} f(d_{ij}) a_j a_i^x, & i \neq j \\ a_j a_i^x, & i = j \end{cases}$ where λ_m is the leading eigenvalue of a square 'landscape matrix' m, in which elements m_{ij} reflect rates of change for the occupancy of patches i (p_i) as a function of patch attributes (often patch area in m^2, a_i and a_j), a dispersal probability function of interpatch distance $f(d_{ij})$ and an extinction probability constant x (commonly set to 0.5).	Hanski & Ovaskainen (2000) (*31*)

Table S2. Forest biome definition used in this study based on the WWF biome classification (*61*).

	Biomes
Tropical forests	Tropical and Subtropical Moist Broadleaf Forests
	Tropical and Subtropical Coniferous Forests
	Tropical and Subtropical Grasslands, Savannas, and Shrublands
Temperate forests	Temperate Broadleaf and Mixed Forests
	Temperate Coniferous Forests
	Mediterranean Forests, Woodlands and Scrub
Boreal forests	Boreal Forests/Taiga

Table S3. Drivers of forest loss based on Curtis et al. (2018) (*8*).

	Driver	Description
Permanent conversion	Urbanization	Forest conversion for the expansion and intensification of existing urban centers.
	Deforestation	Commodity-driven deforestation, defined by the long-term, permanent conversion of forest to non-forest land use such as agriculture (including oil palm), mining, or energy infrastructure, etc.
Temporary transition	Shifting Agriculture	Small- to medium-scale forest conversion for agriculture that is later abandoned and followed by subsequent forest regrowth.
	Forestry	Large-scale forestry operations, such as clearcutting and selective logging, occurring within managed forests with evidence of forest regrowth in subsequent years.
	Wildfire	The burning of forest vegetation with no visible human conversion or agricultural activity afterward.

Table S4. P-value of Kruskal-Wallis test followed by post-hoc Mann-Whitney U tests for fragmentation rate within and outside tropical protected areas.

	All non-protected (ANP)	Matched non-protected (MNP)	Loosely protected (LP)
Matched non-protected (MNP)	<2e-16	-	-

Loosely protected (LP)	<2e-16	0.0096	-
Strictly protected (SP)	<2e-16	<2e-16	<2e-16

990

Table S5. P-value of Kruskal-Wallis test follower by post-hoc Mann-Whitney U tests for fragmentation rate within and outside nontropical protected areas.

	All non-protected (ANP)	Matched non-protected (MNP)	Loosely protected (LP)
Matched non-protected (MNP)	1	-	-
Loosely protected (LP)	0.53024	1	-
Strictly protected (SP)	7.2e-06	0.00018	0.03047

995